Microstructures and reaction mechanisms in biopyriboles

DAVID R. VEBLEN AND PETER R. BUSECK

Departments of Geology and Chemistry, Arizona State University
Tempe, Arizona 85281

Abstract

High-resolution transmission electron microscopy of ferromagnesian chain and sheet silicates from a metamorphosed ultramafic body at Chester, Vermont has revealed a wide variety of structural defects. Images of these microstructures have been interpreted by analogy with images of ordered chain silicates and with the aid of dynamical diffraction and imaging calculations. Most of the defects are concentrated in regions of chain-width disorder; they apparently result from retrograde reaction of anthophyllite to talc and from deformation of the ultramafic body.

The most common defects are the terminations of (010) slabs having a given chain width. These slabs, referred to as "zippers," in most cases terminate coherently, with no displacive planar defects associated with the termination. Two theoretically-derived rules must be obeyed for coherent termination. Rule 1: the terminating zipper must have the same number of subchains as the material it replaces. Rule 2: the numbers of silicate chains in the zipper and in the material it replaces must both be even, or they must both be odd. Where these rules are disobeyed, zipper terminations are usually associated with planar faults having displacements projected on (001) of either ¼ [010] or ¼ [100], referred to an anthophyllite cell. In rare cases, violation of the replacement rules results in severe structural distortion, rather than the creation of displacive planar faults. These replacement rules hold for all pyriboles and may be controlling factors not only in reactions involving amphibole, but in pyroxene hydration reactions as well. Other observed microstructures in the Chester chain silicates include cooperative terminations of many zippers; terminations of individual silicate chains; column defects parallel to the pyribole c axis; narrow lamellae of monoclinic pyribole; and extended displacive faults and rotational faults that apparently result from physical deformation.

Two types of talc have been distinguished by their orientation relationships with the pyriboles. In "coherent talc," the relationship is $b_{tc}||b_{py}$, $a_{tc}||c_{py}$, $c_{tc}||a_{py}$. Structural considerations and high-resolution images suggest that this type of talc possesses $2O$ stacking. In "(210)-talc" there are no rigid orientation relationships with the intergrown pyribole, but the sheets of the talc tend to be parallel or subparallel to (210) of the pyribole. This type of talc displays extreme stacking disorder.

Textural evidence suggests that the wide-chain silicates and fibrous talc at Chester formed by retrograde hydration reaction of anthophyllite. This conclusion is supported by the microstructures observed with electron microscopy. These microstructures suggest that there were several mechanisms for the reaction: (a) anthophyllite and wide-chain pyribole were replaced along grain boundaries and fractures by talc, and (b) anthophyllite was replaced by a far more complex mechanism involving the reaction sequence anthophyllite → disordered chain silicate → chesterite → more disordered chain silicate → jimthompsonite → talc or disordered chain silicate with very wide chains. The disordering steps of this sequence apparently occurred by the nucleation and growth of wide-chain zippers. When a region of crystal achieved a chemical composition close to that of one of the ordered phases, reordering occurred by the passage of *en echelon* termination faults through the structure in the a direction. Much of the chemical transport necessary for these reactions may have taken place by "ultrafast" diffusion along large structural tunnels associated with zipper terminations.

Introduction

It has long been known that biopyriboles may undergo oriented hydration reactions that can transform a pyroxene into an amphibole, or an amphibole into a mica, for example. The former type of reaction, which has been called uralitization, was clearly recognized and described by Goldschmidt (1911, p. 345). Veblen and Burnham (1978a,b) have shown that hydration reaction of amphibole to talc can be accompanied by the production of additional ordered wide-chain silicates, such as chesterite and jimthompsonite, as well as structurally disordered biopyribole having a variety of silicate chain widths.

High-resolution transmission electron microscopy (HRTEM) has been used to elucidate the structure and spatial distribution of ordered and disordered material resulting from the anthophyllite–talc reaction in an ultramafic body at Chester, Vermont (Veblen *et al.*, 1977; Veblen and Buseck, 1979a). The present HRTEM study looks beyond the question of chain-width order and disorder and instead considers the rich variety of structural defects found in the Chester biopyriboles. These defects, which were apparently created during a sequence of metamorphic reactions and deformations in the Chester Dome, can be used to understand the mechanisms of the hydration reactions. Similar textural methods using crystal defects have been used to explore reaction mechanisms in oxide systems (Obayashi and Anderson, 1976).

The structural interpretation of pyribole HRTEM images is now relatively straightforward. The interpretation of defects in the Chester biopyriboles in terms of a reaction model may, however, be open to discussion. Although there is clear textural and microstructural evidence that much of the wide-chain silicate and fibrous talc was formed by hydration reaction from amphibole, there is no rigorous proof that all of it formed in this way; some of the material with triple and wider chains was possibly produced by primary growth. As a result of this ambiguity, we have chosen to present our observations first, with very little interpretation, and then to interpret the observations in terms of a reaction model. The first half of this paper is thus a catalog of microstructures observed in the Chester pyriboles. These include several types of Wadsley defect ("zipper") terminations, stacking faults, partial dislocations, column defects, chain terminations, low-angle grain boundaries, monoclinic lamellae, intergrowths with talc, and phase boundaries. Evidence for the formation of the Chester pyriboles by reaction from amphibole is then summarized, and the above microstructures are used to delineate possible mechanisms for the hydration

reactions. The final section considers mechanisms for the chemical transport that is an integral part of these reaction processes.

This study is part of a broader investigation of biopyribole reactions. Preliminary results on pyroxene hydration reactions indicate that, in some cases, the mechanisms are exactly analogous to the mechanisms described here (Veblen and Buseck, 1978). Our results are thus not restricted to a single locality or even a single mineral group, but may instead prove to be typical of all pyriboles undergoing hydration reaction. Furthermore, microstructures similar to some of those described here are observed in octahedral chain structures, such as manganese oxides (Turner and Buseck, 1979), suggesting even broader applicability of the present work.

Image interpretation and experimental techniques

Veblen and Buseck (1979a) showed that ferromagnesian biopyriboles produce *c*-axis HRTEM images in which dark areas correspond to the positions of the I-beams in the structure. Correlation of such images with diffraction patterns and dynamical diffraction and imaging calculations showed that this relationship holds for a wide range of instrumental conditions and crystal thicknesses; the widths of pyribole I-beams can be recognized in such images. This relationship is further substantiated by defect calculations presented here. Veblen *et al.* (1977) and Jefferson *et al.* (1978) showed that pyriboles also produce interpretable *a*-axis images. Experimental technique and image interpretation for the present work thus follow methods described previously. We assume that the reader who wishes to understand the figures in the present paper will be familiar with those in the earlier work and with the I-beam representation of pyribole structures (Veblen *et al.*, 1977; Veblen and Buseck, 1979a).

The *c*-axis images in this paper were produced from ion-milled specimens, whereas *a*-axis images are from samples that were crushed under acetone and suspended on holey carbon grids. All specimens are from a block of blackwall reaction zone from a metamorphosed ultramafic body near Chester, Vermont, as described by Veblen and Burnham (1978a).

Catalog of pyribole microstructures

"Zippers" and zipper terminations

Silicate chains (and hence I-beams) of the "wrong" width are common in the Chester biopyriboles; they may occur as isolated faults or as broad areas having completely disordered chain widths. Strictly speak-

ing, these chain-width errors are Wadsley defects (Wadsley and Anderson, 1970; Chisholm, 1973) or polysomatic defects (Thompson, 1978), but for the sake of simplicity, we will refer to them here as "zippers," which they resemble in c-axis orientation. The reader is cautioned to not interpret the term zipper as two-dimensional; pyribole zippers are three-dimensional slabs that are usually very extensive in both the a and c directions.

The spatial distribution of chains of various widths has been described by Veblen *et al.* (1977) and Veblen and Buseck (1979a); in this paper we will concentrate on the various ways in which zippers terminate and cooperate with other zippers and with displacive faults of different types. Because the hydration reactions in the Chester pyriboles apparently involve, in part, the growth of wide-chain zippers through the structures, an understanding of the ways in which these zippers terminate is essential to an understanding of the reaction mechanisms.

Coherent zipper terminations. Isolated zippers commonly terminate coherently, without any associated planar defects. The most common zipper width that is observed to terminate coherently in anthophyllite is sextuple. Two distinct types of sextuple zipper terminations are shown in Figure 1a,b, along with I-beam models of the termination structures. The accompanying calculated images confirm the plausibility of these models, which contain large channels running parallel to the c-axis. The calculation method is described in Appendix I.

The minimum dimension of the free aperture[1] (diameter) of the channel in the termination of Figure 1b is about 6.3A, and that in Figure 1a is about 4.8A. These channels are thus enormous compared with the sizes of ions that must diffuse in and out of the structure during hydration reaction; the possible diffusional role of these channels in biopyribole reactions is discussed in the final section of this paper. Presumably these channels are empty or filled to a very low atomic density. Charge-balance considerations suggest that the dangling oxygen bonds that line the channels may be saturated by H^+ ions.

Whereas the fault in Figure 1a has mirror symmetry, the termination in Figure 1b does not, and it appears that the sextuple chains nearest to the large tunnel are not parallel to (100). Instead, in the experimental image it appears that the structure around the channel has relaxed slightly into the defect. The calculated image, however, shows the same effect in its lowermost sextuple-chain I-beam, demonstrating that even a completely unrelaxed model would experimentally appear to be relaxing slightly into the channel. Because the experimental image shows more distortion than the calculated one, and because this relaxation extends for several I-beams into the sextuple zipper, there is probably a small amount of structural distortion around the defect in the real crystal. Since terminations of this type are rare compared to the type shown in Figure 1a, such distortion of the structure is probably energetically unfavorable.

In some cases, coherently terminating zippers have two terminations (Fig. 1c), suggesting that the zippers may have nucleated within the crystal or at the ends of the crystal and grown in both the $+a$ and $-a$ directions.

A number of other chain widths have been observed to terminate coherently in both ordered and disordered pyriboles. Examples involving septuple- and octuple-chain zippers are shown in Figure 1d,e.

Cooperative zipper terminations. In many cases, more than one zipper terminate at the same place. For example, two quadruple zippers may terminate together in anthophyllite (Fig. 2a,b), as may a combination of one quadruple and two triple zippers (Fig. 2c,d). Likewise, the chain sequence (2432522) can turn into the chain sequence (3332423), for example, by cooperation of a number of zippers (Fig. 2e).

Occasionally, a zipper is seen to take a step in the b direction and continue, as in Figure 2f, where a quintuple zipper in anthophyllite jumps 9A parallel to b. This "derailment" can also be thought of as a double and a quintuple-chain zipper replacing a quintuple and a double zipper. Sometimes switches like this are only local, as in Figure 2g,h, and rarely a local switch involves a zipper of an altogether different width (Fig. 2i,j).

Displacive faults at zipper terminations. Although most terminations of zippers are of the coherent types described above, short faults of two different basic types are occasionally observed to connect the terminations of two or more zippers. Such faults are similar to much more extensive displacive faults that are not clearly related to individual zipper terminations; these are described in the section "Extended displacive faults."

The first type of fault is a Wadsley defect or stacking fault with a projected displacement in c-axis images of an integral multiple of ~4.5A in the [010]
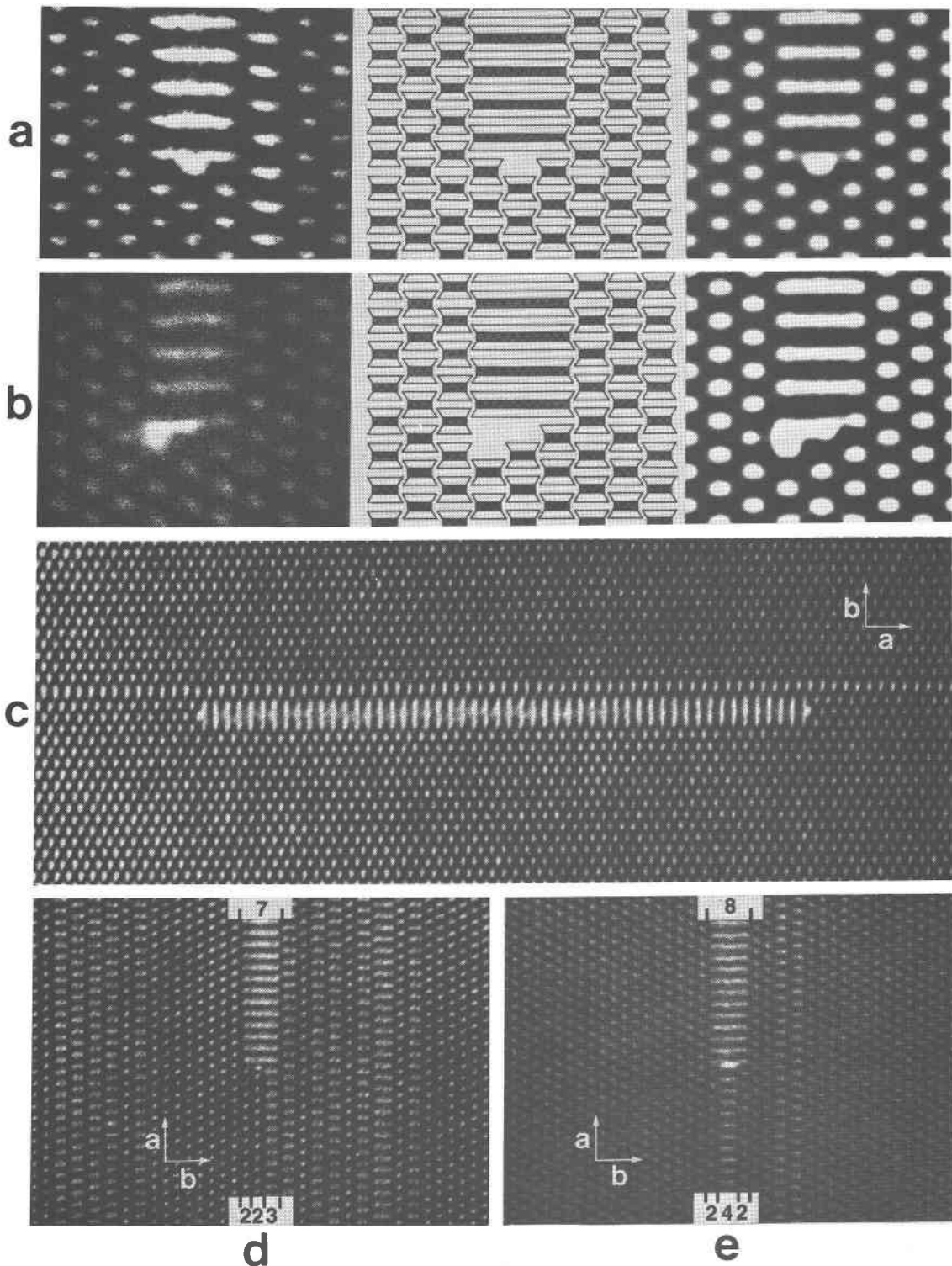
Fig. 1. Simple coherent zipper terminations. a,b: Two different termination types for sextuple-chain zippers in anthophyllite. From left to right are experimental images, models shown in the I-beam representation, and image calculations based on the models. The model and calculation in *a* ignore the triple-chain slab immediately to the right of the sextuple zipper in the experimental image. Scale is given by the double-chain I-beams, which are 9Å in width. The *a* axes are vertical, and *b* axes are horizontal. c: Doubly terminated sextuple zipper. d: Septuple zipper terminating in disordered pyribole. e: Octuple zipper terminating in disordered pyribole.
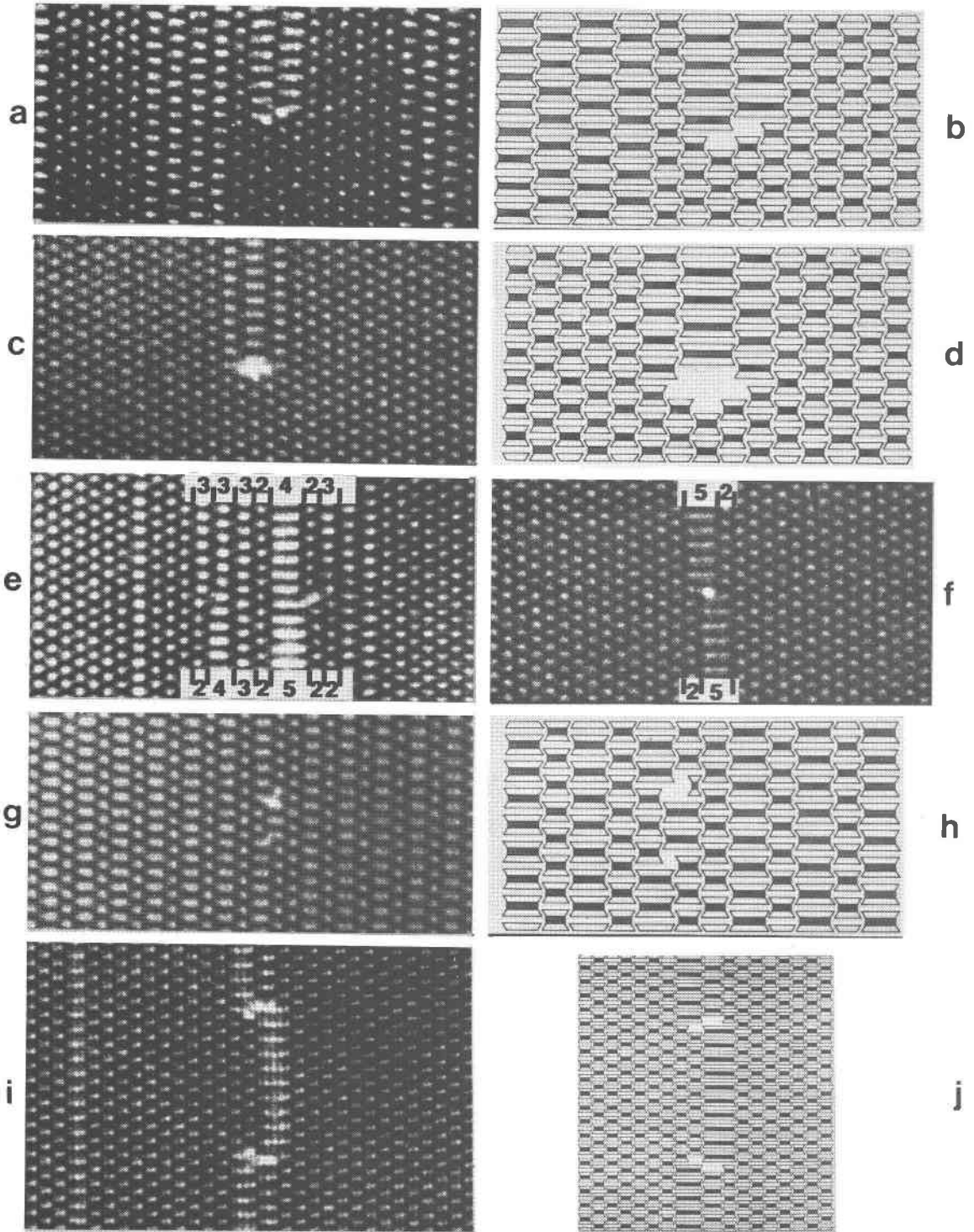
Fig. 2. Cooperative coherent zipper terminations. a,b: Two quadruple zippers terminating together in double-chain material. The I-beam model is not to the same scale as the experimental image. c,d: One quadruple and two triple zippers terminating coherently in anthophyllite. The model is on an expanded scale. e: The chain sequence (2432522) turning into (3332423) by cooperative zipper termination. f: The "derailment" of this quintuple zipper can be thought of as the replacement of the chain sequence (25) by the sequence (52). g,h: Local switching of a double and a triple zipper. The model is at a larger scale. i,j: Local replacement of a double, triple, and quadruple zipper by two double and one quintuple zippers.

direction. The most common orientation of these n/4[010] faults is parallel to the (210) cleavage planes (Fig. 3a).[2] These faults are best described as Wadsley defects, except when they are oriented parallel to (100); they must then be called stacking faults, because the fault vector lies within the plane of the fault.

The second fault type is a Wadsley defect with a projected displacement vector in *c*-axis images of

[2] We have denoted these faults by "n/4[010]" because the projected displacement vector is an integral multiple of one-fourth the anthophyllite *b* axis. Since analogous faults occur in disordered material where the length of *b* is undefined and in jimthompsonite and chesterite, the n/4[010] description is not always accurate. For brevity and simplicity, however, we have chosen to call these faults n/4[010]'s regardless of the structure in which they occur. No such difficulty arises in the case of 1/4[100] faults, since the *a* axes of all orthopyriboles are structurally equivalent.

~4.6A in the [100] direction (Fig. 3b). These planar 1/4[100] defects can have a variety of orientations in the [001] zone, but the most common orientation of the fault plane is parallel to (100). Figure 3c shows both a 1/4[100] and a 1/4[010] fault in their most common orientations cooperating at the terminations of two triple zippers and a quadruple zipper in anthophyllite. Figure 3d is an I-beam diagram of this area, showing the fault structures.

Because rapid electron-beam damage precluded complete determination of displacement vectors by conventional TEM techniques, only the projections of the vectors on (001) could be found experimentally for these displacive faults.

Rules for coherent zipper termination. Two simple theoretical rules governing coherent zipper terminations in biopyriboles can be derived by examining
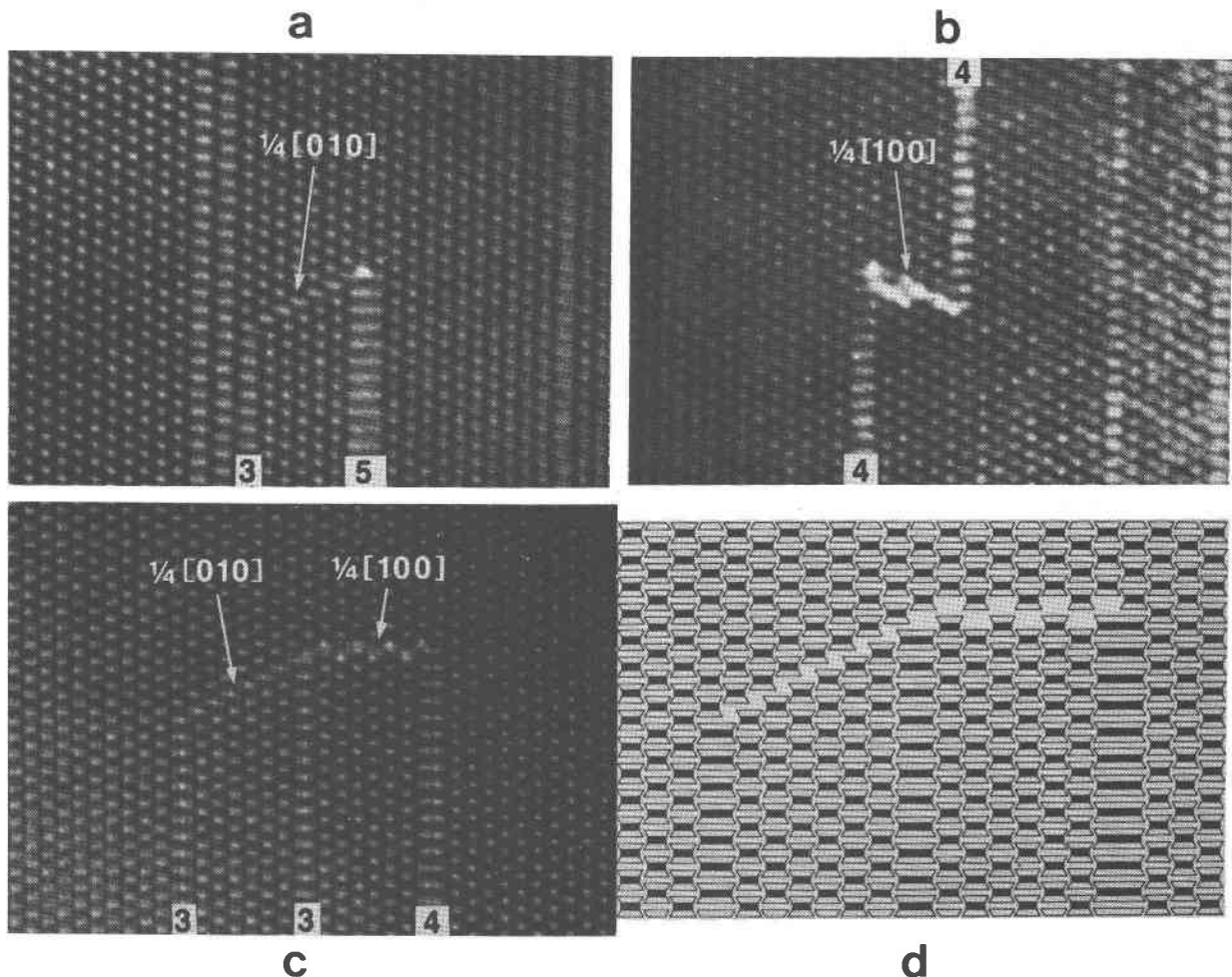
Fig. 3. Displacive faults at zipper terminations. a: A 1/4[010] planar defect connecting a quintuple and a triple zipper terminating in double-chain material. b: A 1/4[100] planar defect connecting the terminations of two quadruple zippers in anthophyllite. The displacement can be determined by measuring between white spots across the fault. c,d: Both types of displacive fault occurring together at the terminations of a quadruple and two triple zippers. The model, which shows the projected displacements and structures for these two types of faults, is on a larger scale than the experimental image.

the structural displacements associated with M and P slabs, as defined by Thompson (1978). The derivation of these rules relies only on the assumption that pyribole I-beams behave as rigid structural modules that cannot be stretched or deformed. Every M or P slab is about 4½A thick in the b direction, and atoms on the $+b$ side of a slab are thus displaced by about 4½A, or $\frac{1}{4}b_{Anth}$, from those on the $-b$ side. If the octahedral cations, for example, are considered, they are not displaced in the a direction from one side of an M slab to the other. In a P slab, however, there is a displacement of about 4½A, or $\frac{1}{4}a_{Anth}$, in the a direction from one side of the slab to the other (see Thompson, 1978, Fig. 3). Each M slab thus produces a structural displacement of $\frac{1}{4}b_{Anth}$, whereas each P slab inherently produces a displacement of $\frac{1}{4}b_{Anth} + \frac{1}{4}a_{Anth}$ in c-axis projection (the displacements parallel to c are complicated by the stacking sequence and are not necessary for this discussion).

When a (010) slab of pyribole structure with one sequence of chain widths is replaced by a zipper or zippers having a different sequence, the total displacements in the original and secondary material must be the same. If not, the new zipper will not connect up with the primary structure on its two sides, and a fault having a displacement equal to the difference between the total displacements in the primary and secondary slabs will result. It is simple to determine whether such a difference in displacements exists for two chain sequences. The total displacement in the b direction is the total number of M and P slabs multiplied by $\frac{1}{4}b_{Anth}$. The total displacement in the a direction is equal to the number of P slabs multiplied by $\frac{1}{4}a_{Anth}$. However, the projected a displacement resulting from two P slabs is equivalent to zero displacement, owing to the translational component of the a glide in orthopyriboles or the a translation in clinopyriboles. Thus, the a displacement associated with an even number of P slabs is always equivalent to zero, and the projected displacement resulting from an odd number of P slabs is always equivalent to $\frac{1}{4}a_{Anth}$.

These theoretical relationships can be stated simply in two rules that are rigorous for all pyriboles, if the I-beams behave as rigid structural modules.

Termination Rule 1: subchain number. The zipper or zippers that terminate must be replaced by structure having the same number of subchains.[3] If the

number of subchains is different, a n/4[010] fault results. This rule is derived simply by noting that the number of subchains in the width of a pyribole slab is equal to the total number of M and P units in the slab.

Termination Rule 2: zipper number. If the number of terminating zippers (of whatever width) is even, then the number of zippers in the material that replaces it must also be even; likewise, an odd number of zippers must be replaced by an odd number. If an odd number replaces an even number or *vice versa*, a ¼[100] fault results. This rule is derived by noting that the number of zippers in a pyribole slab is equal to the number of P modules in the slab. Thus, an even number of zippers results in a net projected displacement of zero in the a direction, and an odd number of zippers results in a displacement of $\frac{1}{4}a_{Anth}$, when viewed down the c axis.

Examination of coherently terminating zippers, whether isolated or cooperating, shows that the above rules are generally obeyed. For example, Rule 1 is obeyed by the sextuple zippers replacing amphibole in Fig. 1a, b, c: three double-chain zippers (a total of six subchains) terminate and are replaced by one sextuple zipper (also six subchains). On the other hand, Rule 1 is violated in Figures 3a and 3c, where triple zippers (three subchains) terminate at faults in amphibole structure (two or four subchains). The second rule is obeyed by the sextuple zippers of Figure 1, because a single sextuple zipper (an odd number of zippers) can coherently replace three double zippers (also an odd number). However, Rule 2 is violated in Figure 3b,c, where one quadruple zipper (odd number of zippers) replaces two double zippers (even number); again, the violating termination is accompanied by a planar fault. Hundreds of examples of the obedience of the coherent termination rules have been observed in the electron microscope. The simple terminations of Figure 1d,e and the cooperative terminations of Figure 2 all obey the rules. Thus, in Figure 2a two quadruple zippers (even number of zippers, total of eight subchains) replace four double zippers (even number, again eight subchains). The replacement of the chain sequence (2432522) by (3332423) in Figure 2e is also in agreement: the number of zippers in each case is seven (odd), and each sequence contains a total of twenty subchains.

The above rules explain several observations in reacting pyriboles. If it is assumed that the Wadsley defects and stacking faults that arise when the rules are violated are energetically unfavorable, then we would not expect to see many examples of zipper terminations that break the rules. This is, indeed, the

---

[3] The number of subchains in a silicate chain is defined as the number of single chains that could be derived by cutting up the structure parallel to (010) (Czank and Buseck, 1980). A pyroxene chain thus has one subchain, an amphibole chain has two, a triple chain has three, and so forth.

case in the Chester pyriboles. These rules also explain why hydration reaction of an augite from the Palisades Sill was observed to begin with the growth of triple-chain zippers into the pyroxene (Veblen and Buseck, 1977; Buseck and Veblen, 1978); one triple zipper (odd number) can coherently replace three pyroxene zippers (also odd). Growth of one double-chain zipper to replace two single-chain zippers would result in a fault of the 1/4[100] type, however, since an odd number of zippers would replace an even number.

An even number of double-chain zippers can, on the other hand, grow into pyroxene together. For example, two double zippers (even number) can coherently replace a slab of pyroxene structure four chains wide (again even). In fact, in orthopyroxene in a harzburgite from Harzburg, Germany, (010) amphibole lamellae contain an even number of amphibole chains almost without fail (Veblen and Buseck, in preparation), presumably because the lamellae grew by migration of coherent zipper terminations and thus had to obey the above rules.

Exceptions to rules for zipper terminations. Although much time has been spent observing the Chester pyriboles with HRTEM, only two exceptions to the above termination rules have been observed. In the first, a triple zipper is transformed to double-chain structure, but without the creation of the expected 1/4[010] fault that should result when three subchains replace two (Fig. 4a,b). Instead, the violation is accommodated by distortion of the structure about a partial dislocation with displacement of ~4.5A in the [010] direction. The resulting fault is thus linear, rather than planar.

In the second case, an octuple zipper replaces four double-chain zippers (Fig. 4c,d). Thus, an odd number of zippers (one) becomes an even number (four), but rather than producing the expected 1/4[100] planar fault, the violation is accommodated by distortion of the octuple I-beams. A given point on one edge of an octuple I-beam is displaced ~4.6A in the [100] direction from the equivalent point on the other edge of the I-beam. The distorted I-beams therefore do not lie with their chains parallel to (100), as is usual in pyriboles.

En echelon termination faults

We observed in some places that pyribole structure with one chain sequence is separated from material with another sequence by a series of faults that are parallel to the orthopyribole (210) or (100) planes. These planar faults are, in fact, cooperative zipper terminations or planar faults, as described above, but rather than being isolated, they occur in groups that are typically arranged *en echelon*. The structure on one side of such a fault group may be disordered, while the structure on the other side is an ordered pyribole. Figure 5 shows a group of *en echelon* faults in material close to chesterite composition. On one side the chain sequence is disordered, while on the other side there is ordered chesterite, with rigorously alternating double and triple chains.

Chain terminations

Much less common than zipper terminations, which do not require individual silicate chains to be broken, are chain-terminating faults that cut across the pyribole c axis. These faults are best observed in a-axis HRTEM images, and they have already been described by Veblen et al. (1977, Fig. 9 and 10) for the Chester pyriboles. Similar chain terminations have also been reported in actinolite (nephrite) by Jefferson et al. (1978).

As reported by Veblen et al., chain terminations usually occur in pairs connected by planar faults having projected displacement vectors of ~4.5A in the [010] direction. Terminations of many chains were also reported to occur at low-angle grain boundaries, which are further described later in this paper. Chain terminations can also change the chain sequence by cooperative switching of two or more adjacent chains; in Figure 6a, the chain sequence (33$\underline{22}$323332223$\underline{232}$32323$\underline{2}$) transforms to (33$\underline{322}$23332223$\underline{332}$2233$\underline{22}$) by the combination of three of these switches. Such chain terminations are not necessarily sharp in a-axis projection, but may take place over several tens of ångströms. The contrast in such faults was interpreted by Jefferson et al. (1978) to result from twisting of the silicate chains. An alternative interpretation is simply that the termination takes place along a line that is not parallel to a, so that in projection the termination appears to be gradational.

In addition to the types of chain terminations cited above, we have also observed one case in which a 9A thick (010) slab of double-chain structure disappears at a partial dislocation (projected fault vector ~9A parallel to [010]) (Fig. 6b). Consideration of the amphibole structure leads to the conclusion that the fault must also entail distortion and an ~4.6A offset parallel to [100] to bring the structure on either side of the inserted slab into registry. This offset is not observed directly, because the displacement direction coincides with the projection direction of the image,
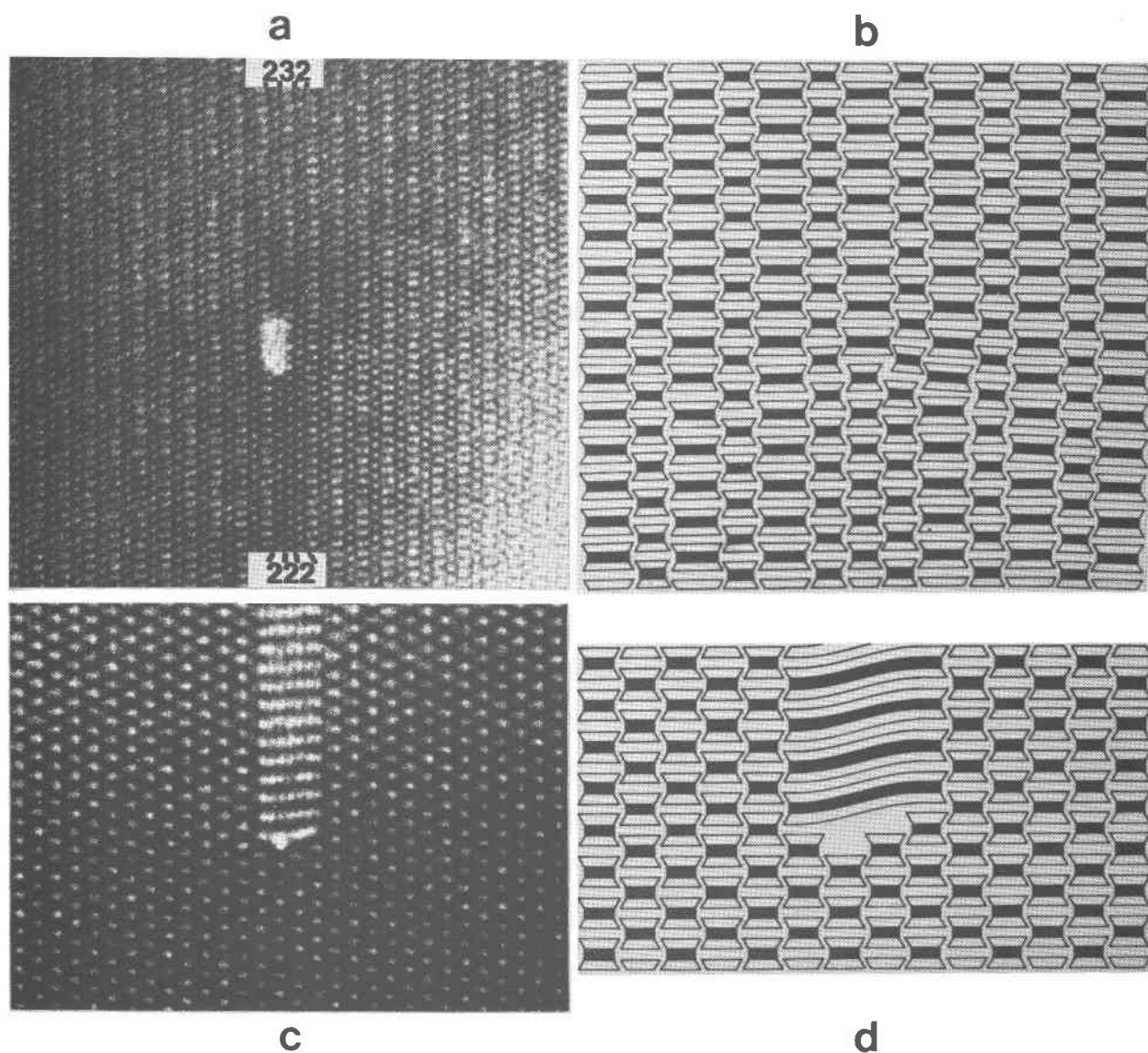
Fig. 4. Violations of chain termination rules. a: A double-chain slab turning into triple-chain material by partial dislocation. The fault can best be seen by viewing at a low angle. b: A model of *a* on a larger scale. The white patch in the experimental image, which was rendered uninterpretable by electron beam damage, may have been occupied by septuple-chain I-beams; it is shown in this model, however, as a simple continuation of the double- and triple-chain structure. c: An octuple-chain zipper terminating in anthophyllite. d: I-beam model of *c*, showing the structural distortion necessary for this type of violation.

but the distortion does result in some strain contrast in the area of the fault.

Column defects

A rare type of defect in the Chester pyriboles appears as a bright white spot in a position usually occupied by an I-beam in *c*-axis images (Fig. 7). Such a fault probably represents a partly or wholly missing I-beam, as shown in the I-beam model. In one instance, a column defect of this sort was located at the termination of an apparent (100) stacking fault. If

these defects do, in fact, represent columns of missing material, they may play an important role in the nucleation of wide-chain material in amphibole.

Extended displacive faults

Another common type of planar fault generally involves a displacement that is an integral multiple of ~4.5A in the [010] direction, with the fault plane typically parallel to the pyribole cleavage. Unlike the n/4[010] faults described above, these faults have not been observed to end at zipper terminations. Since
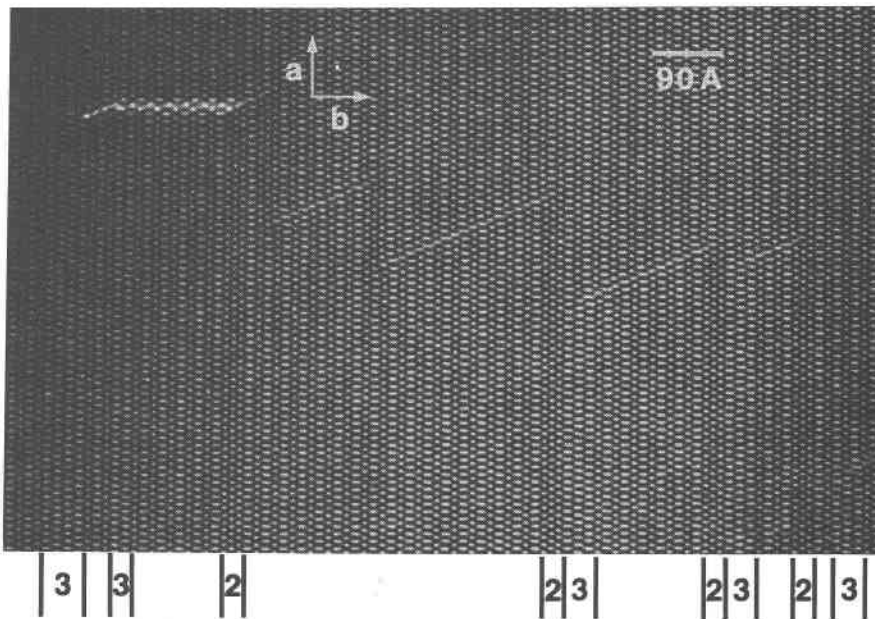
Fig. 5. *En echelon* termination faults. At the top of the figure is perfectly ordered chesterite, which is separated by these faults from disordered pyribole on the bottom. Blocks of structure where double and triple chains do not alternate rigorously are indicated by "2" and "3." The figure is best viewed at a low angle.

recognizable disordered chain sequences are commonly displaced across these faults, they apparently represent planes of fracture along which slip occurred during deformation of the crystal (Fig. 8a, b). These displacements can be as much as several hundred ångströms. In some cases, much of the structure appears to have healed completely after displacement along these faults. In other places, the plane of slippage may be revealed by a series of light spots, probably indicative of incompletely healed structure (Fig. 8b, c). Because these extended displacive faults offset other microstructures (zippers, for example) that predate them, but do not offset microstructures that were formed later, they are important in unraveling the sequence of crystal growth, reaction, and deformation events (see the section "Evidence of reaction from amphibole"). A zipper that grew following the creation of an extended displacive fault may be terminated by the fault, but it will not in general be offset in the manner of a preexistent zipper.

Rotational faults

Another type of fault that apparently results from deformation involves rotation of part of a crystal with respect to another part. Hand specimens show that this sort of deformation took place in the Chester blackwall zone, since some of the chain silicate crystals are severely bent. Veblen *et al.* (1977, their Fig. 9) showed an *a*-axis image of a rotational boundary that cuts across the silicate chains; in that case, the rotation axis was close to *a*. In *c*-axis images we have observed rotational faults in which the axis of rotation is parallel or nearly parallel to *c* (Fig. 9). Similar faults can be observed on a larger scale in thin section with a petrographic microscope. The boundaries between the rotated parts of a crystal can be sharp low-angle grain boundaries, or they can be partially filled with talc (Fig. 9). As with extended displacive faults, the interactions between rotational and other faults can be indicators of event sequences.

Monoclinic lamellae

Occasionally, bands of structure parallel to (100) are observed to have slightly different contrast from that of the surrounding structure (Fig. 10a). Tilting experiments suggest that these are narrow lamellae of monoclinic pyribole, which in most cases are probably analogous to the macroscopic (100) lamellae of cummingtonite, clinojimthompsonite, and the monoclinic analog of chesterite that have been described by Veblen and Burnham (1978a,b).

Although most of the (100) monoclinic lamellae are probably low-Ca pyriboles, some produce diffraction patterns that suggest that their *a* axes are too long to be consistent with this interpretation. Figure
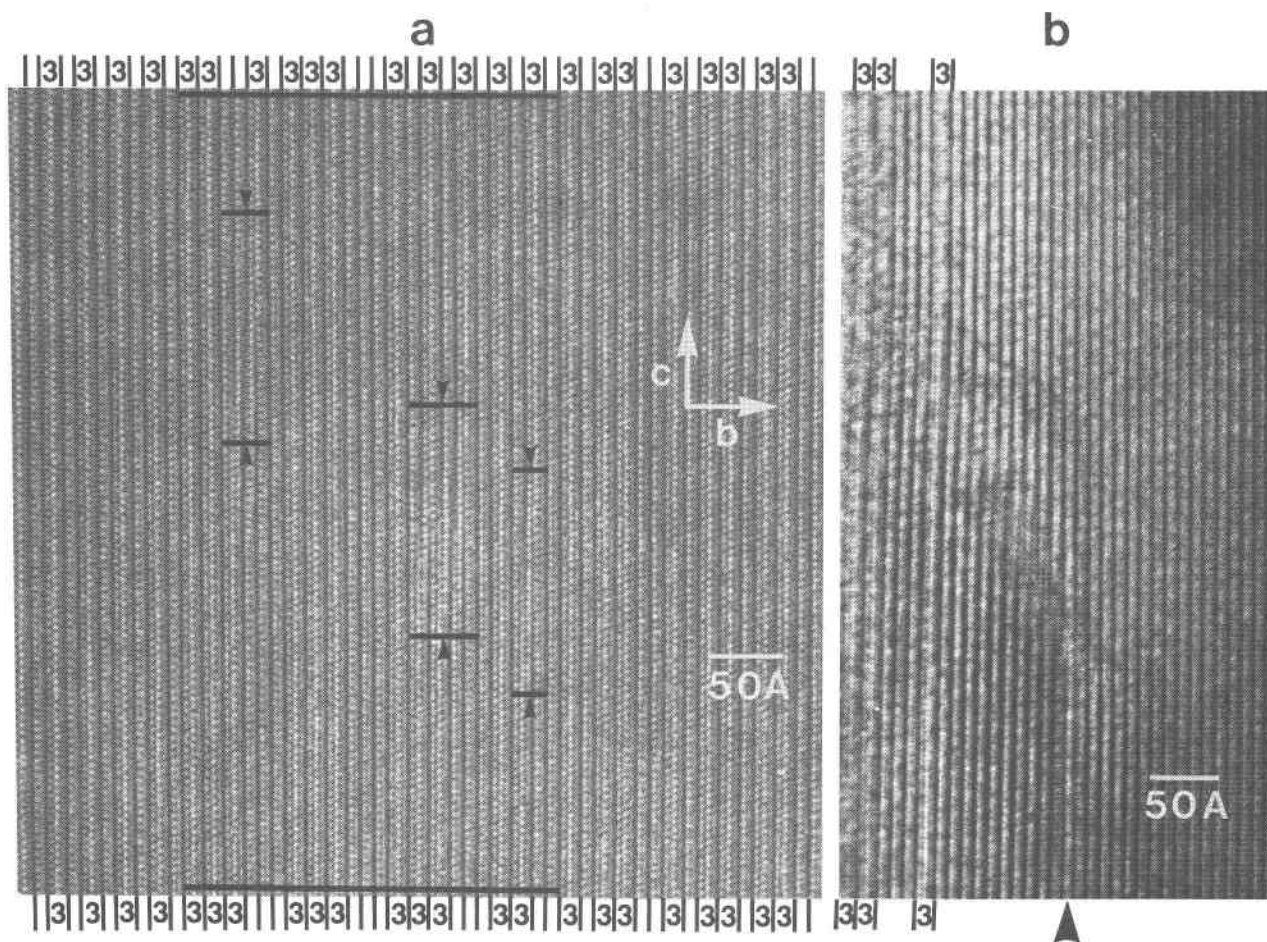
Fig. 6. Chain terminations. a: An *a*-axis image of chain-termination faults changing the chain sequence in double- and triple-chain pyribole. The terminations take place over a considerable projected distance in the *c* direction, and they are best viewed at a low angle. Triple chains are labeled "3" and double chains are unlabeled. b: An *a*-axis image of chain termination at a partial dislocation. A slab of double-chain material (arrowed) disappears, causing structural distortion. Best viewed at a low angle.

10b is the diffraction pattern from the region shown in Figure 10a. Two reciprocal lattices are present, and their values of a^* differ by an amount consistent with identification of the lamellae as actinolite, rather than cummingtonite. Macroscopic (100) intergrowths of anthophyllite and actinolite have been described from the Chester occurrence (Veblen and Burnham, 1978a), and it appears that such intergrowth lamellae can be only a few unit cells wide. No actinolite lamellae were seen with the petrographic microscope in the specimens used in this study, however.

"Flying saucers"

A type of fault that was observed in only a few restricted areas is shown in Figure 11. These faults, which resemble flying saucers in *c*-axis TEM images,
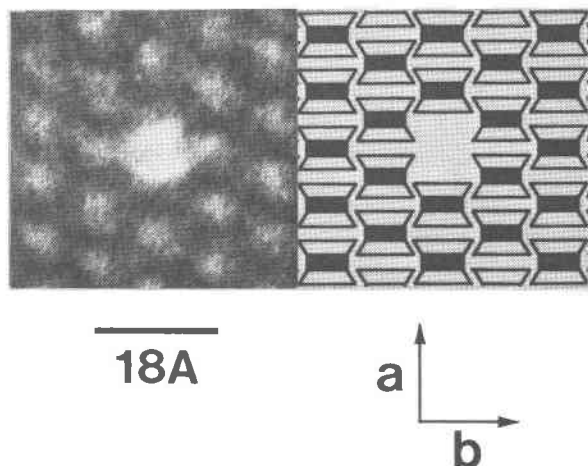

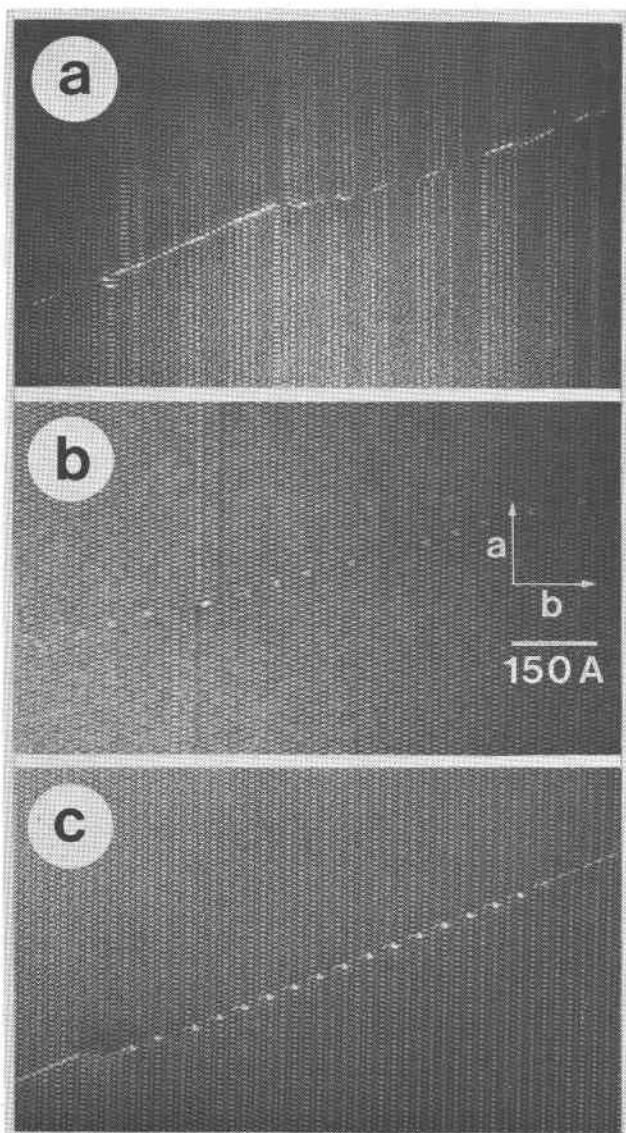Fig. 7. A column defect in anthophyllite, with a model based on a missing I-beam.

Fig. 8. Extended displacive faults. a: In disordered pyribole, showing displacement of the chain sequence across the fault. A few zippers at the left side of the figure are not related across the fault, suggesting that they grew after the displacement occurred. b: In jimthompsonite, showing partial healing of the structure across the fault. Double and quadruple chain-width errors are displaced. c: In perfectly ordered chesterite. The displacement is not an integral multiple of the crystal periodicity, but the structure was able to heal in some places. Best viewed at a low angle.
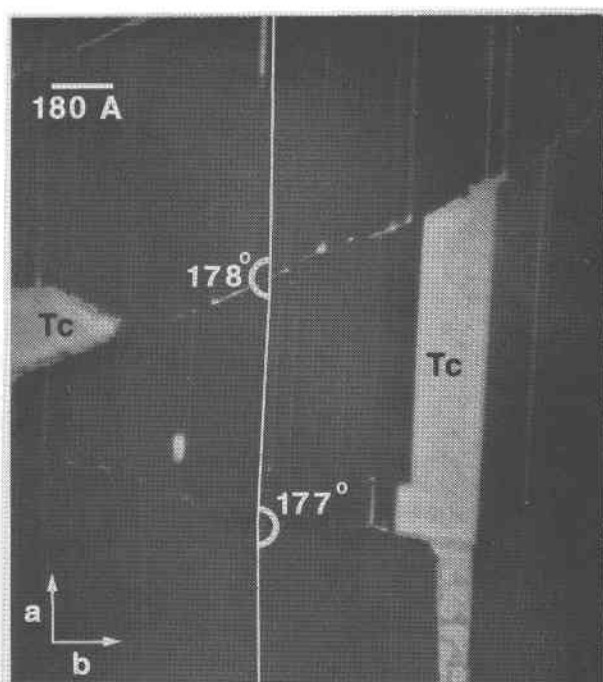

Fig. 9. Rotational faults in disordered pyribole. The fault boundaries can be partially coherent with some zipper terminations or filled with talc (Tc). The vertical white reference line, which is parallel to (010), shows the relative rotations (177° and 178°). Contrast variations result from differences in crystal thickness.

may be epoxy from impregnation during sample preparation), and others appear to have the chain-silicate structure running through them (Fig. 11b), with a contrast change that is consistent with a change in crystal thickness. This last type suggests that the defects were filled with another mineral, which was etched out during alteration or sample preparation. A few images suggest that the bars across some sau-

are diamond-shaped areas a few hundred ångströms wide. They occur in groups (squadrons?) and have boundaries parallel to (210) of the host pyribole. Some of the saucers are separated into two parts by bars of material parallel or subparallel to the pyribole (100) (Fig. 11a). Some of the flying saucers appear to be holes in the crystal, some appear to be at least partially filled with amorphous material (which
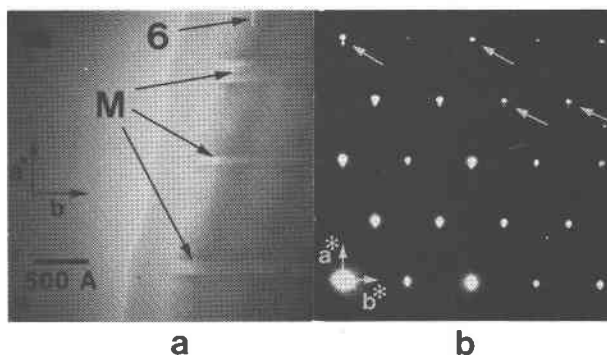

Fig. 10. a: (100) lamellae of monoclinic amphibole (M) in anthophyllite. A sextuple zipper (6) terminates coherently in the anthophyllite. b: Electron diffraction pattern from region shown in *a*. Splitting of diffractions (arrowed) indicates a difference in a^* that suggests the lamellae are high-calcium amphibole.
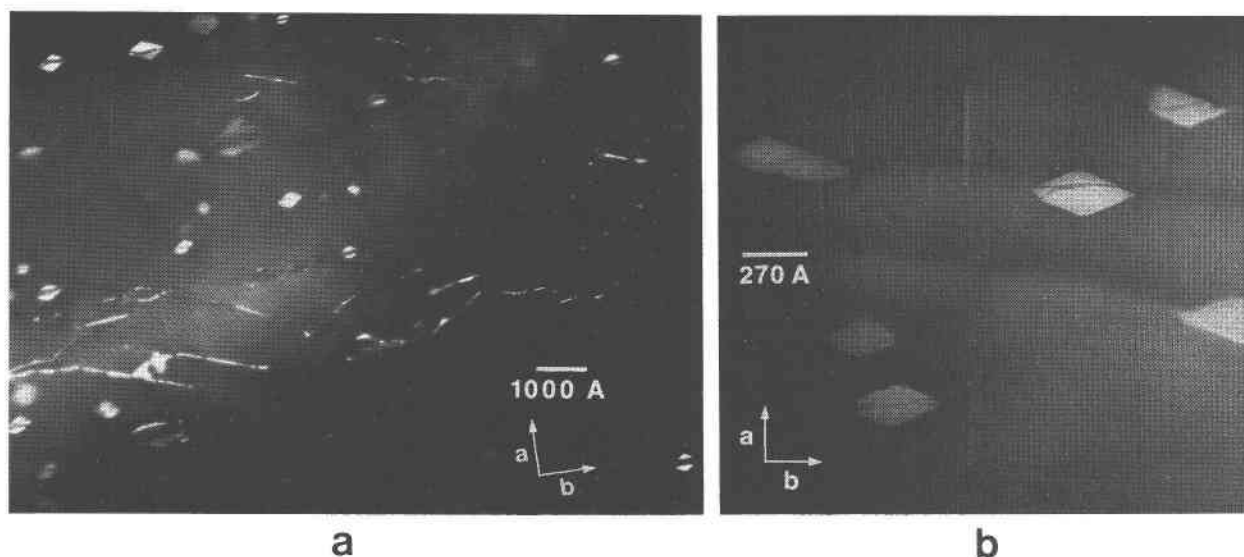
a   **b**

Fig. 11. "Flying saucers." a: In anthophyllite. Some of the saucers have bars running through them parallel to (100). b: In disordered chesterite. The pyribole structure is visible across the defects, and the contrast change is consistent with a change in specimen thickness; the saucers may be pits that were occupied by another phase that has been etched away. Strain contrast emanates from the corners of some of the saucers.

cers may be talc. There is weak strain contrast associated with the saucers in Figure 11b, indicating mild deformation of the pyribole in the neighborhood of the defects. Although flying saucers are uncommon in the Chester material, and their chemical and structural properties are still unresolved, analogous unidentified objects have also been spotted in altered pyriboles from other localities (Veblen and Buseck, in preparation).

Talc

Talc is observed macroscopically in two different forms in the Chester blackwall zone. Primary massive talc is found with actinolite in the innermost zone of the blackwall, whereas fibrous talc occurs as a pseudomorph after chain silicate (Veblen and Burnham, 1978a). In this paper, we shall be concerned only with the fibrous talc that occurs in intimate association with the ferromagnesian pyriboles and with the textural and microstructural relationships between talc and the chain silicates.

Talc is ubiquitous in the TEM specimens studied, occurring along grain boundaries, between the parts of rotationally faulted crystals, and intergrown with the chain silicates in various ways. Using HRTEM, many sheet silicates can be recognized by the spacing of the (00*l*) fringes that they produce when viewed parallel to the layers (Veblen and Buseck, 1979b) and, in some, by the common bending of these layers. Although microchemical analyses were not avail-

able, the sheet silicate observed in this study was identified as talc by its 9.3A basal spacing and by comparison with images of talc that had first been identified in petrographic thin section. Another striking feature of talc that separates it from the true micas is the rapid rate with which it suffers electron beam damage. Whereas talc is rendered amorphous after a few seconds in the electron beam, some of the sheet silicates with interlayer cations can be observed for several minutes. Though an aid to recognition, the rapid beam damage of talc makes HRTEM observations very difficult.

Stacking order and disorder. Streaking of electron diffraction patterns in the direction of c^* indicates that areas of talc large enough for selected-area diffraction have severe stacking disorder (Fig. 12, inset). In addition to the major 9.3A basal fringes, some high-resolution images have the light fringe broken up into a series of spots, as described by Iijima and Buseck (1978) for biotite. By analogy with the magnesian pyriboles with empty A-sites, these white spots presumably correspond either to the interlayer sites or to positions between these sites, depending on focus (see Veblen and Buseck, 1979a, Fig. 3). In either case, the positions of these spots from layer to layer can be used to infer the degree of stacking order (Iijima and Buseck, 1978).

A detailed treatment of the stacking possibilities in talc would be quite complex, because the stacking vectors need not lie on the mirror planes of the indi-
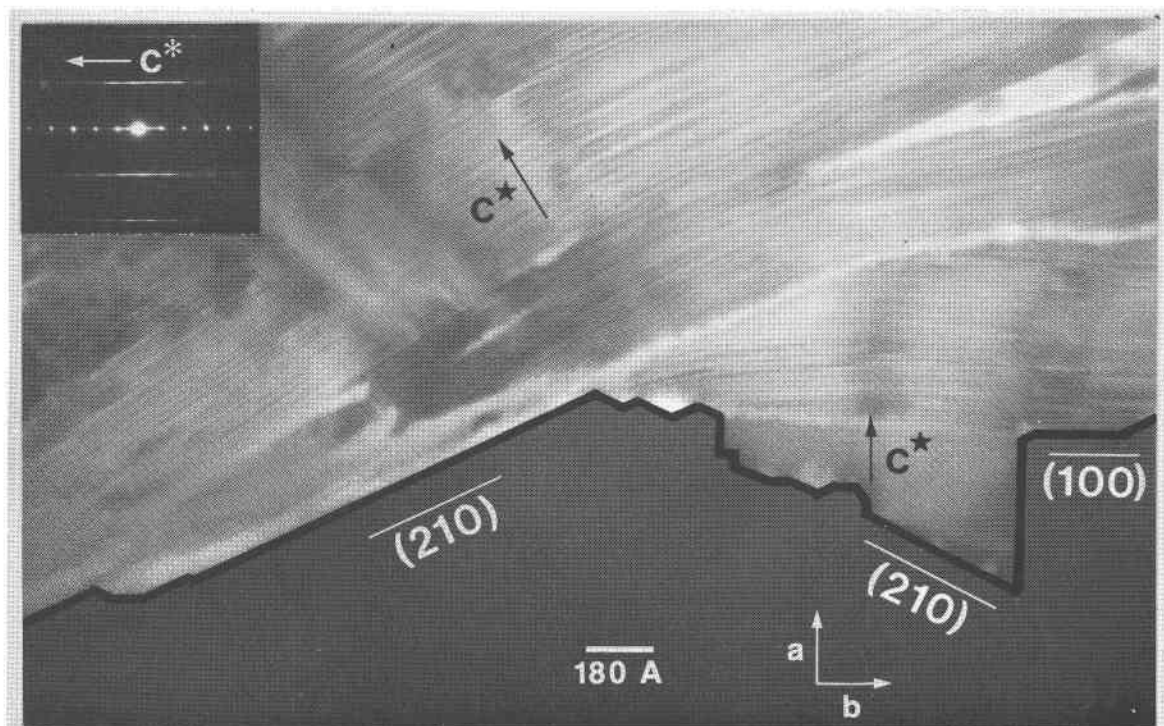
Fig. 12. Orientation relationships between talc (lighter material with fringes) and anthophyllite (darker material). Some of the talc has its (00*l*) fringes parallel or subparallel to the (210) planes of anthophyllite. Talc that is constrained by chain silicate has its sheets nearly parallel to the anthophyllite (100) planes and *c** parallel to the anthophyllite *a* axis. The electron diffraction pattern, which shows heavy streaking characteristic of stacking disorder, is from the (210)-talc.

vidual TOT layers (Rayner and Brown, 1973; Ross *et al.*, 1968). However, a qualitative distinction can be drawn between two different types of talc in the Chester material:

(1) Talc in which the white spots in the image fall on straight lines parallel to *c**. This is consistent with the distribution of interlayer sites found in 2*O* (or 1*M*) stacking. The stacking sequence 2*O* is analogous to the ++−− stacking of orthopyriboles and is presumably the type of stacking found here, since this type of talc is usually observed to occur as small areas embayed on at least three sides by orthorhombic pyribole (Fig. 12). In order for the interface to be coherent, the talc stacking must be 2*O*. In this case, the pyribole and talc *b* axes coincide, as do the pyribole *a* axis and the talc *c* axis. This type of talc could just as well be called very wide chain silicate, since its sheets typically terminate at planes parallel to (010). The material far from the chain edges is certainly talc-like, however, since it suffers rapid electron damage and often has deformation and dislocation features that are also typical of larger grains of talc (see below).

Talc with ordered stacking was not observed by Akizuki and Zussman (1978) in their HRTEM study of several massive and fibrous talc specimens. They suggested that talc with stacking order may not occur; our observations suggest, however, that ordered talc can grow in limited amounts during the replacement of chain silicates.

(2) Talc in which the white spots in the image do not fall on straight lines parallel to c^*_{talc}, indicating disordered stacking. In large enough areas, this type of talc produces diffraction streaking in the *c** direction. Disordered talc is usually not structurally constrained by pyribole on three or four sides. Instead, it typically occurs along pyribole grain boundaries and sometimes bears no obvious orientation relationships to surrounding chain silicates, although the talc sheets are frequently parallel or subparallel to the orthopyribole (210) planes (Fig. 12).

Talc microstructures. Individual TOT layers of Chester talc are commonly observed to terminate at dislocations having displacement vectors of ~9.3Å in the [001]* direction. Loss of a layer is easily accommodated in the talc structure by deformation of the sheets. Several layers sometimes terminate together, with accompanying deformation of the surrounding structure (Fig. 12, 13, 16a).

A much less common type of defect in the talc in-

volves the intercalation of an extra layer ~5A thick between the 9.3A TOT layers (Fig. 13). We believe that the 5A layer is most likely an extra layer of octahedral cations, similar to a brucite sheet. Such a defect would be similar to the intercalation of a slab of chlorite structure, which has alternating TOT and brucite-like layers. A theoretical basis for such a defect is described by Thompson (1978). Figure 13 shows the termination of the extra layer, along with the termination of several talc sheets.

Talc–pyribole relationships

(210)-talc. As noted above, much of the fibrous talc with stacking disorder is oriented with its sheets parallel, or nearly so, to the (210) planes of adjacent orthorhombic pyribole crystals. Some of the talc in Figure 12 is of this type, which we shall call "(210)-talc." It occurs in contact with anthophyllite, chesterite, jimthompsonite, or disordered pyribole. The (210)-talc is generally in close contact with the chain silicate, but in places it appears to have pulled away at the phase boundary, perhaps during specimen preparation. This suggests that the interface between (210)-talc and pyribole crystals is not as strong as the bonding between individual talc sheets, which are less commonly pulled apart.

Where the talc is not rigorously parallel to the orthopyribole (210) planes, talc TOT layers are seen to terminate at the interface. Even where the talc is rigorously parallel to (210), however, one or more layers have been observed to terminate at ledges in the interface (Fig. 14). Formation and migration of such ledges could well be an important mechanism for the growth of (210)-talc from chain silicate, as discussed
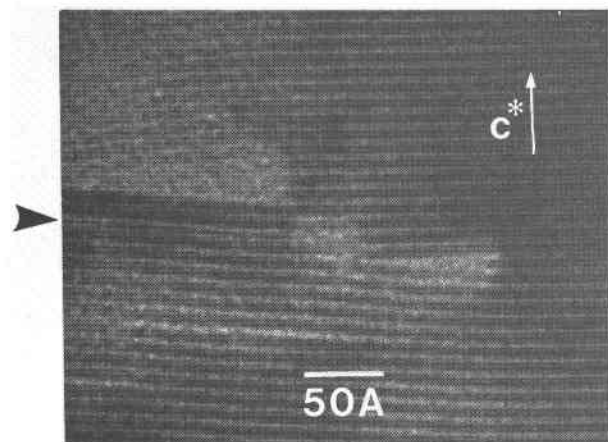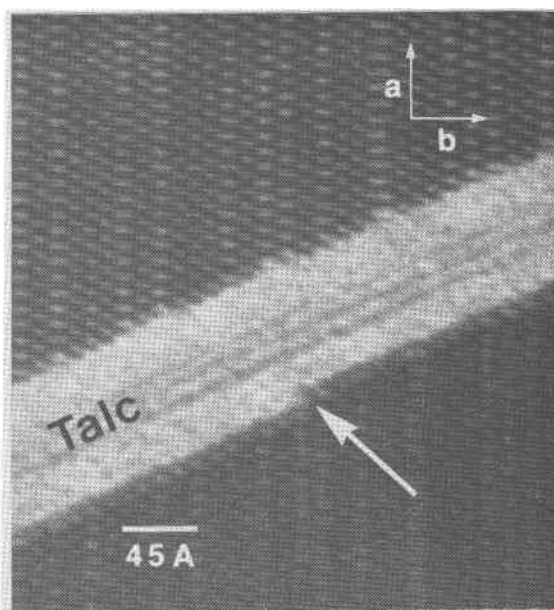

Fig. 14. A ledge (arrowed) in the interface between disordered pyribole and (210)-talc. The talc is apparently growing along a displaced fracture parallel to the pyribole cleavage.

in the section "Mechanisms of anthophyllite–talc reaction."

Coherent talc. Much of the talc that is intergrown with the chain silicates has its *b* axis parallel or subparallel to the pyribole *b* axis and has its *c** parallel or nearly so to the pyribole *a**, as discussed in the section "Stacking order and disorder." Occasional bending and termination of TOT layers upset these orientation relationships locally, but the talc–pyribole interfaces usually remain coherent. We therefore shall refer to this type of talc as "coherent talc."

Much of the coherent talc is observed to contact the chain silicates only on planes parallel to (010). This talc thus appears simply as zippers with very wide chains running through pyribole with narrower chains; there is, of course, a continuum of structures between what we call chain silicate and talc. The sheets of some of these very wide zippers are not strictly parallel to the (100) planes of the host pyribole. Other very wide zippers commonly exhibit bending of the layers (Fig. 15), another trait that we generally associate with talc rather than chain silicate. Some very wide zippers of talc have been observed to extend for large distances in pyribole crystals without terminating or changing width; they are not obviously concentrated in the vicinity of grain boundaries.

In regions near grain boundaries, small areas of talc are sometimes embayed in pyribole. Coherent

Fig. 13. An extra 5A layer (arrowed) and its termination in talc. The extra layer is probably a brucite-like sheet, producing a local configuration similar to the chlorite structure.
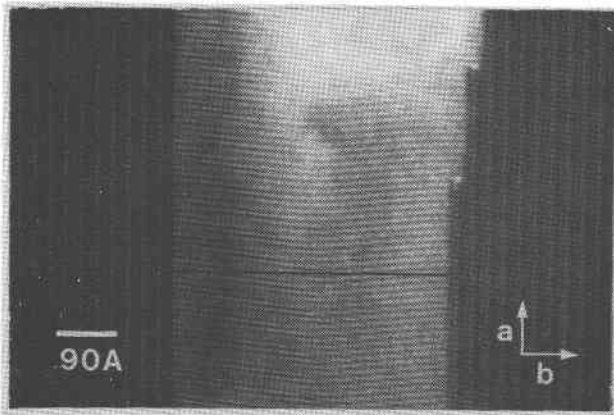
Fig. 15. Bending of the layers of a very wide (talc-like) zipper in chesterite. The straight horizontal black line is for reference.

talc also commonly occurs directly on the grain boundary, with very wide zippers extending a short distance into the pyribole and then terminating. The coherent talc near grain boundaries can be in contact with the various ordered and disordered pyriboles not only on planes parallel to (010), but also in other orientations, most commonly the pyribole (100) and the orthorhombic pyribole (210). Examples of coherent talc exhibiting the three most common boundary orientations are shown in Figure 16.

Structural models of the common types of talc–pyribole boundaries are illustrated in Figure 17; the chain silicate used in these models is anthophyllite, but analogous boundaries are also observed with chesterite, jimthompsonite, and disordered pyribole.
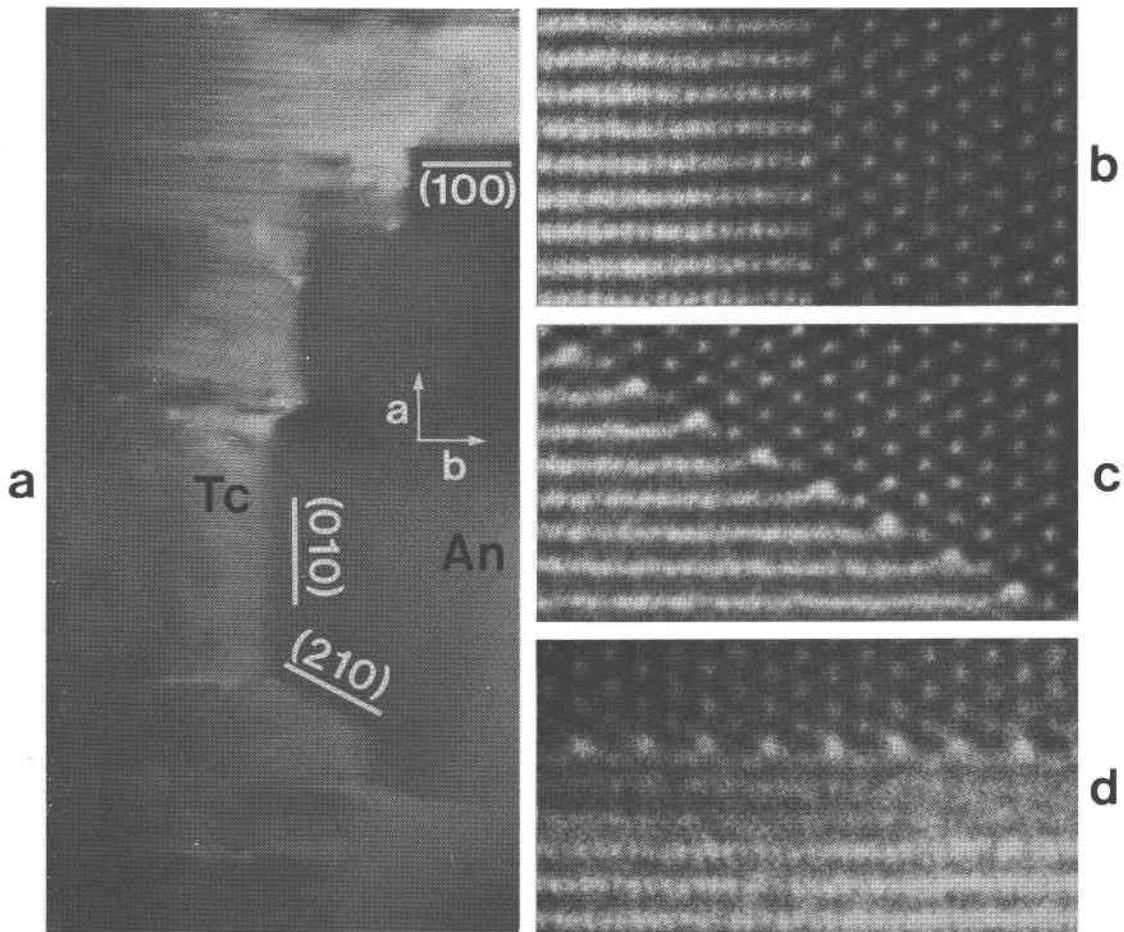

Fig. 16. Embayed coherent talc exhibiting the three most common boundary orientations. This intergrowth is with anthophyllite, but analogous boundaries also occur with other pyriboles. a: Overview showing orientations in terms of pyribole axes. b: A (010) boundary. c: A (210) boundary. d: A (100) boundary.
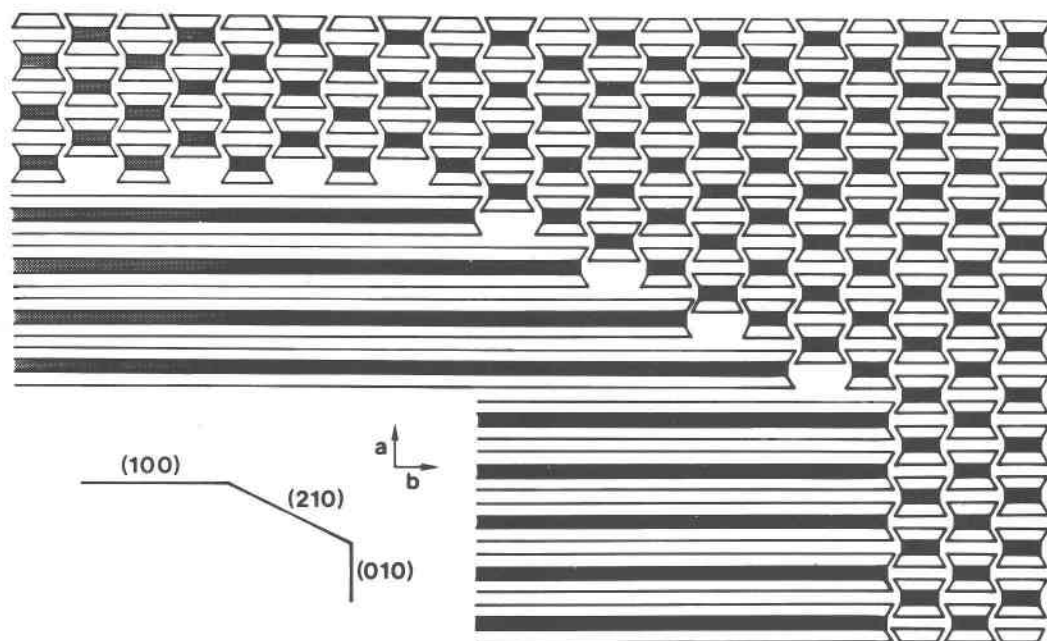
Fig. 17. I-beam model showing the three common types of coherent talc–pyribole boundary. The (010) boundary consists of "normal" biopyribole structure (a P slab), while the other two orientations entail large tunnels running parallel to the pyribole c axis. Boundary orientations in terms of pyribole axes are given in the inset.

The structure of the (010) boundary model is simply that of a P (pyroxene) slab, as defined by Thompson (1970, 1978). With respect to first- and second-nearest neighbor coordinations, such a boundary therefore is similar to ordinary pyribole or talc structure. The (100) and (210) boundary models, on the other hand, contain tunnels that are structurally dissimilar to any part of a normal ordered biopyribole structure (Fig. 17). These channels, like those found at some zipper terminations, contain dangling bonds along the I-beam edges. These dangling bonds, which are perhaps satisfied by H^+, would likely cause (100) and (210) boundaries to be energetically less favorable than (010) boundaries; this relationship might then account for the much greater frequency of (010) boundaries.

Even less common than (100) and (210) pyribole–talc boundaries are those with other orientations or with many steps in them. In general, these other boundaries can be thought of as being made up of sections of the three boundary types shown in Figure 17. Very rarely, other more unusual types of boundaries are observed. Such an abnormal talc–chesterite interface is shown in Figure 18, in which the contrast is not of the sort normally produced by biopyriboles in c-axis orientation. The structure of the boundary therefore cannot be interpreted with reliability. This

image may result from rotation of the talc sheets so that they are not parallel to the pyribole chains in the neighborhood of the boundary. Such a boundary would presumably be structurally discontinuous.

Evidence of reaction from amphibole

Macroscopic and petrographic evidence

The textures and sequence of phases in the Chester blackwall zone have been described by Veblen and
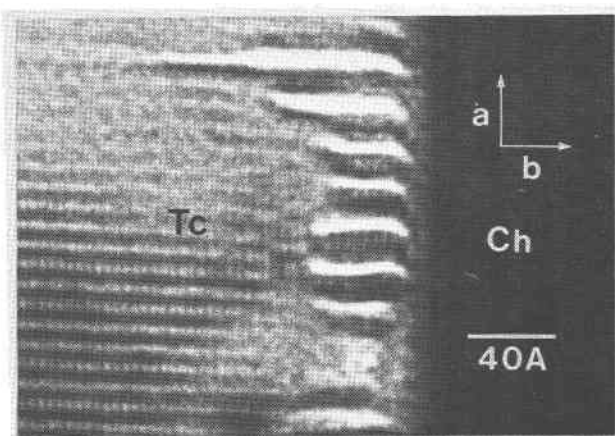

Fig. 18. An unusual talc–chesterite interface. The image is uninterpretable in terms of normal biopyribole structure and may result from twisting of the talc sheets near the interface.

Burnham (1978a); here we summarize the evidence relevant to the origin of the fibrous talc and discuss further evidence that has been derived from HRTEM. In hand specimen, fibrous talc appears as an obvious pseudomorph after chain silicate. Individual "crystals" may consist of pyribole at one end and talc at the other, and the talc may retain the clear prismatic external morphology of the original amphibole, as shown by Phillips and Hess (1936, Fig. 6). In places, sprays of fibrous talc penetrate into the chlorite zone, cutting across the layers of the chlorite (Fig. 19a); the low-Ca pyriboles, where they have not been replaced by fibrous talc, cut the chlorite in the same way. In other places, patchy islands of pyribole that are optically in a single orientation are separated by fibrous talc (Fig. 19b); these islands are presumably rema-

nent pieces of an amphibole crystal that was continuous before partial replacement by talc.

Closer to the interior of the ultramafic body, individual "crystals" may consist of low-calcium amphibole at one end and actinolite at the other. Between their ends, such crystals consist of a fine intergrowth of anthophyllite and actinolite on planes near (100); the actinolite contains cummingtonite lamellae exsolved on (001) (I-centered cell setting), as shown in Figure 19c. Anthophyllite crystals are commonly divided in two by a single straight crack parallel to (100) (see Veblen and Burnham, 1978a, Fig. 2a). Such cracks are reminiscent of the common herringbone twin planes of monoclinic amphiboles and pyroxenes, and because such twinning is precluded by the space-group symmetries of orthorhombic pyri-
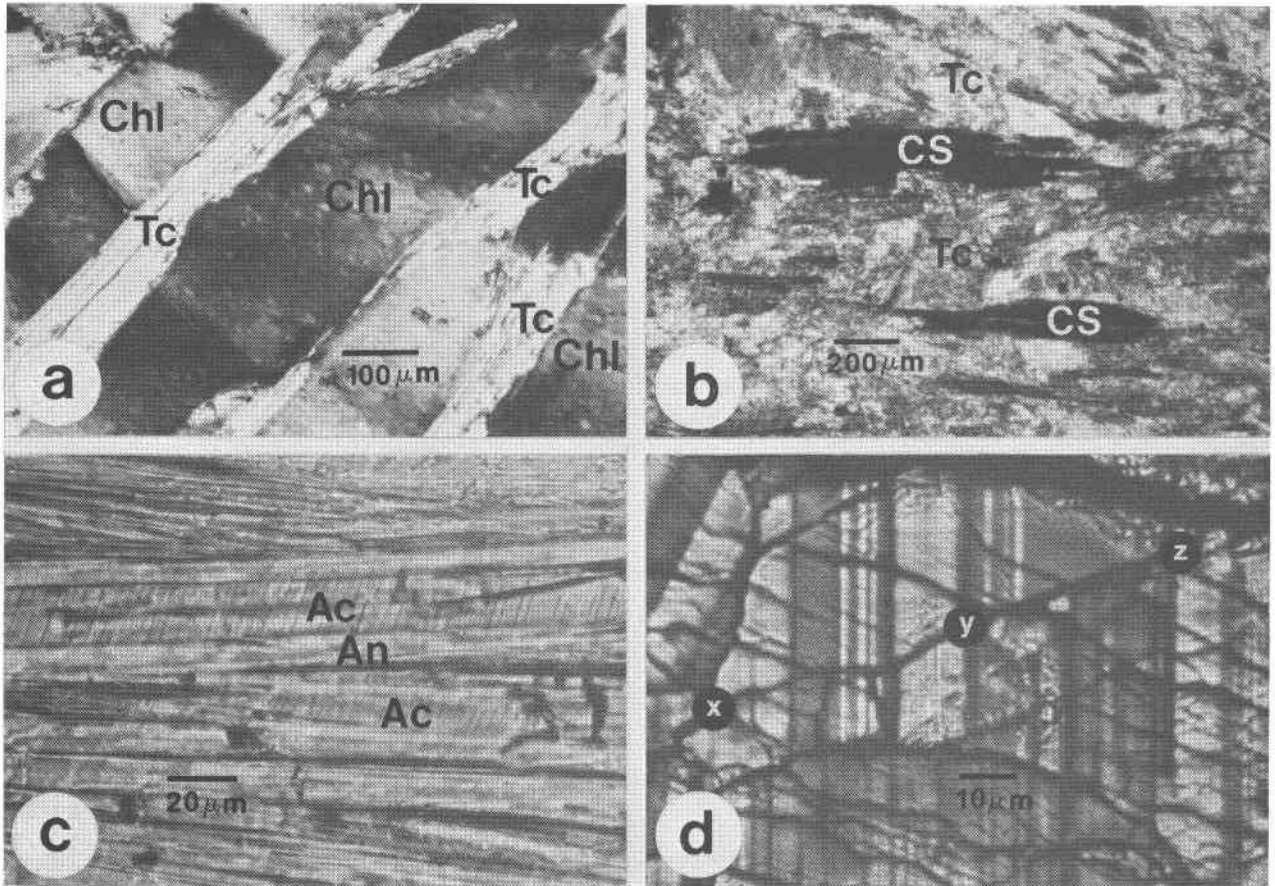

Fig. 19. Petrographic micrographs of Chester biopyriboles. a: Fibrous talc (Tc) penetrating chlorite (Chl) in a manner typical of amphibole in other parts of the blackwall zone. The sprays of fibrous talc cut across the chlorite sheets. Crossed polars. b: Islands of chain silicate (CS) in optical continuity and embayed in fibrous talc. The islands appear to be remanents of the pyribole–talc reaction. Crossed polars. c: Intergrowth of actinolite and anthophyllite on planes near (100). The actinolite contains (001) exsolution lamellae of cummingtonite (I-cell setting). Plane polarized light. d: Relationships of polysomatic lamellae of ordered and disordered pyribole across a fracture. The lamellae are continuous across the fracture between x and y, but discontinuous between y and z. This suggests that the lamellae between x and y grew prior to the fracture, whereas those between y and z postdate the fracture. Crossed polars.

boles, the cracks suggest that the crystals were originally monoclinic. These textures lead to the conclusion that the Chester anthophyllite is itself a reaction product forming pseudomorphs after high-calcium amphibole. In fact, actinolite is much more typical than anthophyllite as a blackwall phase (Phillips and Hess, 1936; Chidester, 1967), and even at Chester actinolite is apparently the only chain silicate in much of the blackwall.

Textural evidence from thin sections of the polysomatic intergrowths is also suggestive of a reaction origin for the wide-chain pyriboles. In (001) sections, polysomatic lamellae are commonly observed to terminate at fractures. In some cases, the lamellae terminate along part of a fracture but are not terminated along other parts of the same break, as shown in Figure 19d. Such relationships imply that the fracture existed prior to the growth of at least some of the wide-chain lamellae. Where lamellae cross the fractures, the two parts of the crystal must have been in close structural contact at the time of reaction, while the growth of the polysomatic lamellae was terminated in places where cracks already existed.

Microstructural evidence

The microstructural evidence for the production of the wide-chain silicates from amphibole largely follows the same lines as some of the petrographic evidence, but it extends this evidence to a much smaller scale. Veblen *et al.* (1977, their Fig. 9) showed a rotational fault in anthophyllite, along which many triple and quadruple chains terminated. They argued that the creation of the fault must have predated the formation of the triple and quadruple chains, because the wide chains were not rigorously correlated across the fracture. Similar reasoning can be applied to zipper terminations at rotational faults and extended displacive faults.

Figure 20 shows a large area of anthophyllite with triple and wider zippers that is crossed by displacive fractures. This bright-field low-resolution image was taken with *c* tilted a few degrees away from the microscope axis to enhance contrast of the wide chains at low magnification (~17,000× initial magnification). The wide-chain zippers are rigorously correlated, but offset by ~130A, across one of the faults ("A"), indicating that the fault formed after the growth of the wide-chain material. Across another fault ("B"), however, the zippers are not related to each other, implying that the amphibole crystal was faulted before the growth of the wide chains. Other faults display an intermediate relationship, in which
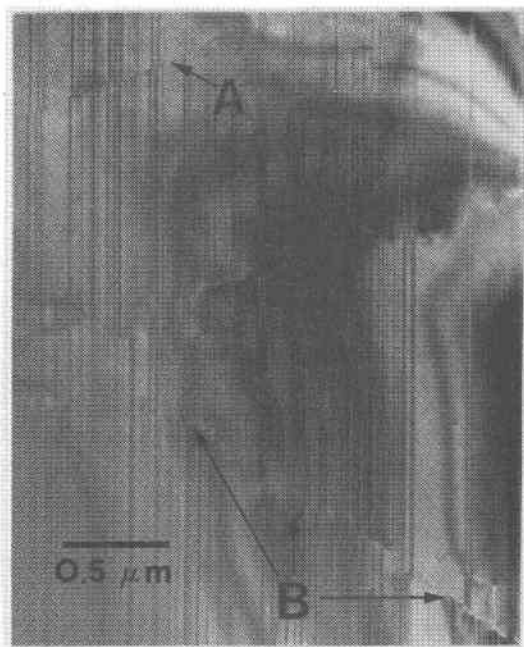

Fig. 20. Low-resolution single-beam bright field image of anthophyllite with chain-width disorder. The chain-width errors (vertical stripes) are rigorously correlated across fracture A, but not across fracture B, indicating that they formed after B but before A.

some of the zippers match across the fracture, while others do not (Fig. 8a, for example). Larger lamellae of ordered wide-chain pyribole have similarly been seen to either terminate at such fractures or merely be displaced by them. These relationships show that deformation of the Chester ultramafic body, which probably is responsible for the creation of these extended faults, occurred before, during, and after the growth of wide-chain material.

Rotational faults observed in *c*-axis images can likewise be used to argue that an amphibole crystal existed before the growth of wide-chain material. In Figure 9, for example, most wide-chain zippers terminate at the fault boundaries. These rotational faults presumably result from physical deformation, with the fracture openings in some cases filling with secondary talc. It is also possible that some of these rotations actually result from the reaction process itself; if part of a crystal reacts to a wide-chain silicate and then develops a stable (210) crystal face, material must be removed by dissolution, and part of the crystal must rotate as the resulting space closes under pressure. Such rotations of parts of multiphase pyribole crystals can be observed in thin section.

The textural and mineralogical relationships in the Chester wall zone, both macroscopic and microscopic, suggest that structurally ordered amphibole

was the primary chain-silicate phase. Initial growth of actinolite was followed by reaction to low-calcium amphiboles, which in turn reacted to wide-chain pyriboles and fibrous talc. Caution must be exercised in interpreting all the features of this mineral occurrence in terms of reaction from amphibole, however. As pointed out by Veblen and Buseck (1979a), the textural evidence does not rule out the possibility that small amounts of wide-chain silicate could have grown as primary crystallization products in opening fractures, for example. Nevertheless, since most of the microstructures described in this paper are pervasive, at least in regions exhibiting chain-width disorder, they can be interpreted in terms of a reaction model. Conversely, the details of the retrograde reaction of the low-calcium amphibole can be deduced from these microstructures.

Mechanisms of anthophyllite–talc reaction

Direct replacement by (210)-talc

The simplest mechanism of reaction from anthophyllite to talc is direct replacement by (210)-talc. This mechanism merely involves reaction at grain boundaries or along fractures. Such replacement can affect not only structurally ordered anthophyllite, but also chesterite, jimthompsonite, and disordered pyribole, which are first produced by mechanisms described below.

The growth of (210)-talc apparently takes place by the migration of growth ledges at the talc–pyribole interface (Fig. 14). These ledges can be one or more talc TOT layers high. Once nucleated, such a ledge would tend to migrate, consuming chain silicate and producing talc, since talc is the more stable low-temperature phase. In thin section, much of the fibrous talc is oriented with its sheets parallel to (210) of partially consumed orthorhombic pyribole, suggesting that the direct growth of (210)-talc from chain silicate is volumetrically an important mechanism of reaction at Chester.

Direct replacement by coherent talc

Like (210)-talc, much of the coherent talc is concentrated near grain boundaries and fractures. Coherent talc presumably nucleates at the edge of the pyribole crystal and then grows into the pyribole (in three dimensions, even embayed coherent talc may well have been connected to a crystal surface). The growth may take place preferentially on the relatively unstable pyribole (210) and (100) interfaces, which have numerous dangling bonds (Fig. 17). The

(010) interfaces, on the other hand, consist of rather normal structure for biopyriboles, and can thus be expected to be relatively stable. The notion that growth proceeds primarily in the pyribole a direction is consistent with the observation that coherent talc areas are frequently much longer parallel to a than they are parallel to b. However, this elongation may simply be the result of the greater stability of (010) boundaries, rather than the kinetics of their growth.

Coherent replacement by zipper migration and reordering

By far the most complex mechanism of reaction involves the replacement of anthophyllite by other ordered and disordered pyriboles and finally by talc. This mechanism has been discussed in general terms by Veblen and Burnham (1975, 1976, 1978b), Veblen and Buseck (1979a), and Veblen et al. (1977); anthophyllite is successively replaced by disordered material having triple or wider chains, chesterite, more disordered material, jimthompsonite, still more disordered material, and finally talc. In this section, we discuss specific mechanisms by which these replacements may occur.

Disordering of anthophyllite. The first step in the formation of wide-chain material in anthophyllite is nucleation. The double termination of some wide-chain zippers in anthophyllite (Fig. 1c) suggests that in some cases they nucleated either within the anthophyllite or at one end of the crystal. Following rapid propagation parallel to the chain direction, they grew in the +a and −a directions. Column defects (Fig. 7) may, in fact, represent nucleation events of this sort. Likewise, the concentration of wide-chain zippers near some grain boundaries suggests that nucleation on grain boundaries also occurred. In either case, the nucleation of zippers with coherent terminations must follow the rules for coherent zipper termination. Similarly, zippers that break these rules could nucleate cooperatively with the simultaneous creation of displacive faults connecting their terminations.

Once a wide-chain zipper (or group of cooperating zippers) has nucleated and attained some critical size, it should grow, consuming anthophyllite, if the material in the zipper is thermodynamically more stable than anthophyllite. With falling metamorphic temperature, wide-chain material may well become more stable than double-chain silicate, once conditions have left the range for anthophyllite stability and have become appropriate for the stability of talc (or wide-chain silicates, if they are stable). Expansion of

a zipper into anthophyllite can be accomplished by dissolution of ions of the anthophyllite at the termination and by recrystallization of these ions into the material with wider chains. This process must be coupled with diffusion of octahedral cations out of the crystal and diffusion of H^+ in, as discussed further in the next section. It is not known, of course, whether the removed and deposited ions are individual atoms or whether they are larger clusters, such as SiO_4^{4-} groups or even larger blocks of structure, as suggested by Eggleton (1975) for hedenbergite → nontronite reactions. We can guess, however, that in these hydration reactions, the destabilizing effect of H^+ or H_2O on Si–O bonds (Burnham, 1975; G. V. Gibbs, personal communication) may be important. Hydroxylation occurring along channels at zipper terminations could catalyze the breakup of existing structure.

As a simple example of zipper migration, let us examine the expansion of a single slab of sextuple-chain material into anthophyllite. As shown earlier (Fig. 1a, b), sextuple zippers are observed to terminate in two distinct ways. With the most common termination type, the zipper could expand as shown schematically in Figure 21. Most of the material involved in this expansion needs to move only a few ångströms. The rate of such a zipper growth mechanism is probably controlled by the rate of breakup of the parent structure and the rate of diffusion of a relatively small number of octahedral and H^+ ions (the reaction step diagrammed in Figure 21 requires removal of only 9.5% of the octahedral cations). Possibly under suitable conditions a sextuple zipper could zip through anthophyllite quite rapidly in this way, given rapid diffusion along the channel and structural breakup catalyzed by H^+. The second termination type in Figure 1 suggests that a zipper can expand by more than one mechanism. Different termination types could alternate along the termination in the *c* direction, and through time. All observed zipper terminations, both simple and cooperative, involve channels and, presumably, unsatisfied bonds. These similarities suggest that the mechanisms of zipper expansion are at least similar in all cases.

The spatial distribution of wide-chain zippers and associated displacive faults in anthophyllite is not homogeneous. Instead, these reaction features are concentrated in certain parts of a crystal, while large areas of the same crystal may be perfect anthophyllite. Figure 22 shows two such areas of concentrated defects that we interpret to be in the first stages of reaction toward talc. Material like this commonly occurs between anthophyllite and areas with extreme chain-width disorder. The distribution of defective and perfect anthophyllite indicates that the reaction is initiated quite locally. The chemical or physical parameters responsible for the initiation of reaction are not understood. Possibly, once an area has started to react, minor structural stresses resulting from the defects further destabilize the anthophyllite nearby. Alternatively, the pattern of reaction may be controlled by externally imposed chemical potential variations, for example.

Ordering and disordering of chesterite and jimthompsonite. Once a disordered part of a crystal has attained a composition near that of chesterite, it may transform into the chesterite structure. This can occur by the passage through the structure of *en echelon* termination faults like those in Figure 5. The chain sequence on one side of such a fault is different from that on the other side, and movement of the faults in the *a* direction causes replacement of one structure by another. If the disordered material has exactly the chesterite composition, then only local chemical transport is required for this transformation. Such a
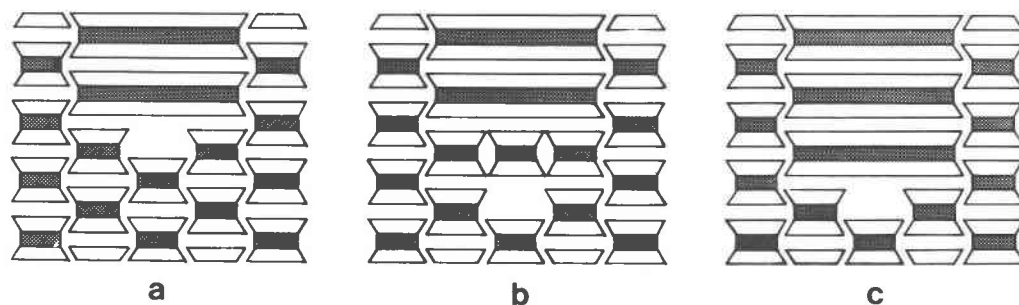

Fig. 21. I-beam diagrams schematically showing a possible mechanism for the expansion of a sextuple zipper in anthophyllite. a: Initial configuration. b: Most of the material in one I-beam moves upward about 5Å. The I-beam representation oversimplifies this step because the distorted octahedral sites are not shown. c: Final configuration, after diffusion of small numbers of octahedral cations and H^+, and healing of the structure.
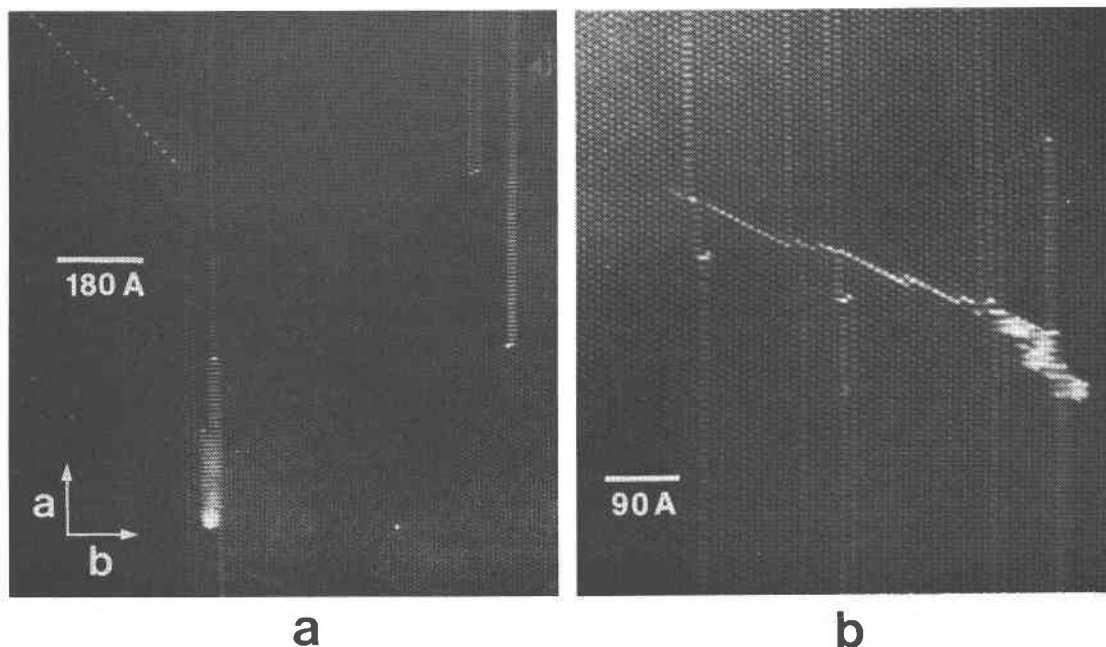
Fig. 22. Two areas in anthophyllite in the initial stages of reaction by zipper growth. Zipper terminations and associated displacive faults typically occur in groups. a: In undeformed area of anthophyllite. b: Along a partially healed extended displacive fault resulting from crystal deformation.

transformation could also occur piecemeal, by the expansion through the structure of cooperating zippers; over a period of time, a more ordered state could be approached.

Because chesterite occurs as macroscopically observable, well-ordered lamellae, it can be assumed that once part of a crystal has ordered to chesterite, it will remain in this state for some time. Eventually, however, it may begin to react to jimthompsonite. This reaction follows lines analogous to those for anthophyllite reacting to chesterite. Again, we have nucleation and growth of wide-chain zippers with the attendant diffusion of octahedral cations and H$^+$ that changes the chemical composition toward that of talc. As the composition approaches jimthompsonite, ordering again occurs by the passage of faults through the structure in the a direction. The result of this reordering is the jimthompsonite structure, which has only triple chains.

In some parts of the Chester blackwall, jimthompsonite replaces anthophyllite directly, without ordering into chesterite as an intermediate step. In this situation, the first ordering transformation must occur as the composition nears that of jimthompsonite. Possible phase relations responsible for these different types of behavior during the reaction are discussed by Veblen and Buseck (1979a).

Reaction to talc. There are several mechanisms by which jimthompsonite finally reacts to talc. The growth of (210)-talc at the expense of pyribole occurs throughout the reaction sequence, as outlined above, and much of the jimthompsonite is converted to talc in, or near, this orientation. Jimthompsonite is also susceptible to replacement by coherent talc near grain boundaries and fractures. Finally, the replacement of jimthompsonite by very wide chains, which can proceed by the nucleation and growth of wide zippers, can eventually result in talc. To date, ordering into large areas of quadruple-chain or even wider-chain silicates has not been observed. In a few places, the association of three of four quadruple chains has been observed, but this could easily result from the random placing of chains of various widths. This ordering behavior is vastly different from that of single, double, and triple chains, which form macroscopically ordered crystals. Ordered pyriboles having quadruple and wider chains may, of course, form elsewhere under appropriate conditions.

Mechanisms of chemical transport

The diffusion of cations in silicates is generally a sluggish process, especially at the relatively low temperatures of the retrograde metamorphism at Chester (below about 650° for the reactions described in this paper). Because the anthophyllite–chesterite–jimthompsonite–talc reactions require compositional

change, and hence diffusion in and out of the reacting crystals, normal vacancy-hopping diffusion mechanisms would require the reactions to be very slow. Is there some other mechanism, however, by which the chemical transport could be much more rapid and permit zipper migration to proceed at a reasonable rate?

Although diffusion in silicates is usually slow, there are some structures in which it can be extremely rapid, most notably where there are large tunnels present. Such rapid interstitial diffusion (Peterson, 1968) is responsible for the cation exchange properties of some zeolites, for example; without the very rapid movement of cations in and out of the structure, such exchange would not occur on a practical time scale (Barrer, 1978, p. 256). Similarly, "ultrafast" diffusion by interstitial mechanisms has been observed in a number of metallic systems (Peterson, 1968; Dyson *et al.,* 1966, 1967; Dyson, 1966). In tetragonal (white) tin at room temperature, for example, the diffusion coefficient of copper is as much as 10^{12} times greater than the self-diffusion coefficient of tin (Dyson *et al.,* 1967). This gross difference results because the diffusion of copper is by an interstitial mechanism, while the tin moves by a vacancy-hopping mechanism. There are tunnels in the tetragonal tin structure through which copper atoms can move rapidly and, in fact, the diffusion coefficient is strongly anisotropic, with the fastest diffusion occurring in the tunnel direction. There is little question that in both silicates and metals, diffusion can be extremely fast along structural tunnels that are large with respect to the diffusing species.

Structural models for all observed zipper terminations include tunnels running parallel to c, most of which have minimum free aperture diameters of about 4.8A (see Fig. 1a,b; 2a,b; footnote 1). In some cases, the tunnels are even larger (Fig. 1b). The probability that these models are correct has been demonstrated by comparison of experimental and calculated images (Fig. 1a,b; Appendix I). Since diffusion of cations as large as Rb occurs rapidly in zeolites with channels only 2.6A in diameter (Breck, 1974, p. 579), it is likely that diffusion along zipper terminations is still more rapid, especially at metamorphic temperatures. By analogy with zeolites, the ion exchange required for zipper expansion can conceivably take place on time scales of minutes, suggesting that the diffusional constraint on the growth of zippers may not even be significant. Furthermore, most of the cations do not need to move in or out of the structure at all. Conversion of a P slab ($M_4Si_4O_{12}$) to an M slab [$M_3Si_4O_{10}(OH)_2$] requires that only one-fourth of the octahedral cations diffuse out and that twice as many H^+ ions diffuse in. Since anthophyllite is one-half M slabs to begin with, the complete conversion to talc only requires that one-seventh of the octahedral cations be removed. Most of the other ions need not move more than about 5A for zipper expansion. The growth of zippers could thus be a very rapid process, controlled primarily by the rate of breakup of the parent structure and the rate of recrystallization into the zipper.

Similar reasoning can be applied to the reordering of disordered pyribole into chesterite or jimthompsonite by the passage through the structure of *en echelon* termination faults. In this case as well, there are large tunnels along the faults, and if the parent structure composition does not quite match that of the structure that replaces it, adjustments could take place rapidly along the tunnels. Even where the bulk compositions of the two structures are the same, diffusion parallel to b is necessary for reordering to occur, but again, ions could probably move rapidly along the faults. Most of the material, however, must only move a few ångströms for the termination faults to migrate through the crystal.

Diffusion rates probably pose no problems for the growth of (210)-talc, because cations could easily move along the sheet terminations of the growth ledges and along the talc–pyribole interface. The case of coherent talc growing in chain silicate is more complex, however. Figure 17 shows that a model of a (010) interface contains no large tunnels, whereas interfaces with other orientations do. Growth of talc at the expense of pyribole at a (010) interface thus requires ordinary "lattice" diffusion of cations in talc and chain silicate, and would therefore be relatively slow. With the benefit of rapid diffusion along large channels, the other types of interface could be expected to migrate much faster. This is consistent with the observation that the smallest dimension of coherent talc regions is generally in the b direction. However, as discussed above, the elongation of the talc regions may simply be the result of the greater stability of the (010) interfaces.

Conclusions

Ferromagnesian biopyriboles from a metamorphosed ultramafic body near Chester, Vermont, contain a rich variety of microstructures. These have been characterized by high-resolution transmission electron microscopy. Textural and microstructural evidence indicate that the biopyriboles evolved

through the reaction sequence actinolite → anthophyllite → chesterite → jimthompsonite → talc, with pyriboles having chain-width disorder entering the sequence between the ordered phases.

When the observed microstructures are interpreted in terms of a reaction model, a complex picture of the reactions emerges. Any of the low-calcium pyriboles can react directly to talc along grain boundaries or fractures. Alternatively, anthophyllite can react successively to chesterite and jimthompsonite by the solid-state conversion of double-chain material to material with wider chains, followed by reordering involving the passage of faults through the structure. The growth of wide-chain silicate probably occurs by the expansion of Wadsley defects, or "zippers." Large structural tunnels at the terminations of these zippers may permit the reactions to proceed at reasonable rates by providing pathways for ultra-fast diffusion.

Appendix I. Method of defect image calculation

The defect image calculations of Figure la,b were computed with the SHRLI programs (O'Keefe *et al.*, 1978) as previously applied to ordered biopyriboles by Veblen and Buseck (1979a). Since the method of calculation is only suitable for periodic structures, calculation of nonperiodic defects is performed by constructing large unit cells containing the defect surrounded by a substantial amount of the host structure. The defect calculation is thus not exact, but is equivalent to sampling and Fourier transforming the diffuse diffracted intensity arising from the defect at many discrete points in reciprocal space. The pseudo unit cells used for the calculations of Figure 1 are slightly larger than the areas shown.

A computer program was written to compute atom positions in *c*-axis projections of large defect cells. Using input consisting of the widths and center coordinates of the I-beams, this program constructs the M (mica) and P (pyroxene) parts of the biopyribole structure, preserving the polyhedral geometries and linkage details of I-beams in real Mg,Fe biopyriboles, as determined from structure refinements.

After calculation of the atom positions, computation proceeded as described by Veblen and Buseck (1979a), using the same instrumental parameters. For the calculations of Figure 1a and 1b respectively, there were 2878 and 2924 atoms in the unit cells. Potential functions were formed from 12400 Fourier coefficients for each defect structure, 3097 diffractions were used in the multislice dynamical diffraction calculations, and final images were formed by 2721

beams accepted by the objective aperture. Crystal thicknesses were 53A.

The calculated images of Figure 1 show that intuitive interpretation of biopyribole *c*-axis defect images is successful; as in the ordered structures, dark areas correspond to I-beam positions. Unfortunately, computation time for dynamical imaging of structures with large unit cells is extensive; for this reason, further computations were not performed for other defects. Central processor time for each of the calculations in Figure 1 exceeded three hours on a Univac 1100/42.

References

Akizuki, M. and J. Zussman (1978) The unit cell of talc. *Mineral. Mag., 42,* 107–110.

Barrer, R. M. (1978) *Zeolites and Clay Minerals as Sorbents and Molecular Sieves.* Academic Press, London.

Breck, D. W. (1974) *Zeolite Molecular Sieves.* Wiley, New York.

Burnham, C. W. (1975) Water and magmas: a mixing model. *Geochim. Cosmochim. Acta, 39,* 1077–1084.

Buseck, P. R. and D. R. Veblen (1978) Trace elements, crystal defects, and high resolution electron microsopy. *Geochim. Cosmochim. Acta, 42,* 669–678.

Chidester, A. H. (1967) Evolution of the ultramafic complexes of northwestern New England. In E-an Zen, W. S. White, J. B. Hadley and J. B. Thompson, Eds., *Studies of Appalachian Geology: Northern and Maritime,* p. 343–354. Wiley-Interscience, New York.

Chisholm, J. E. (1973) Planar defects in fibrous amphiboles. *J. Mater. Sci., 8,* 475–483.

Czank, M. and P. R. Buseck (1980) Crystal chemistry of silica-rich barium silicates. II. Electron microscopy of barium silicates containing multiple chains. *Z. Kristallogr.,* in press.

Dyson, B. F. (1966) Diffusion of gold and silver in tin single crystals. *J. Appl. Phys., 37,* 2375–2377.

———, T. Anthony and D. Turnbull (1966) Interstitial diffusion of copper and silver in lead. *J. Appl. Phys., 37,* 2370–2374.

———, ——— and ——— (1967) Interstitial diffusion of copper in tin. *J. Appl. Phys., 38,* 3408.

Eggleton, R. A. (1975) Nontronite topotaxial after hedenbergite. *Am. Mineral., 60,* 1063–1068.

Goldschmidt, V. M. (1911) Die Kontaktmetamorphose in Kristianiagebiet. *Vidensk. Skrifter, I. Mat.–Naturv. Klasse,* No. 1.

Iijima, S. and P. R. Buseck (1978) Experimental study of disordered mica structures by high-resolution electron microscopy. *Acta Crystallogr., A34,* 709–719.

Jefferson, D. A., L. G. Mallinson, J. L. Hutchison and J. M. Thomas (1978) Multiple-chain and other unusual faults in amphiboles. *Contrib. Mineral. Petrol., 66,* 1–4.

Obayashi, H. and J. S. Anderson (1976) Solid state reactions in the system $Nb_2O_5 \cdot WO_3$: an electron microscopic study. *J. Solid State Chem., 19,* 331–351.

O'Keefe, M. A., P. R. Buseck and S. Iijima (1978) Computed crystal structure images for high resolution electron microscopy. *Nature, 274,* 322–324.

Peterson, N. L. (1968) Diffusion in metals. In F. Seitz, D. Turnbull and H. Ehrenreich, Eds., *Solid State Physics, 22,* p. 409–512. Academic Press, New York.

Phillips, A. H. and H. H. Hess (1936) Metamorphic differentiation at contacts between serpentinite and siliceous country rocks. *Am. Mineral., 21,* 333–362.

Rayner, J. H. and G. Brown (1973) The crystal structure of talc. *Clays and Clay Minerals, 21,* 103–114.

Ross, M., W. L. Smith and W. H. Ashton (1968) Triclinic talc and associated amphiboles from Gouverneur mining district, New York. *Am. Mineral., 53,* 751–769.

Thompson, J. B., Jr. (1970) Geometrical possibilities for amphibole structures: model biopyriboles. *Am. Mineral., 55,* 292–293.

——— (1978) Biopyriboles and polysomatic series. *Am. Mineral., 63,* 239–249.

Turner, S. and P. R. Buseck (1979) Manganese oxide tunnel structures and their intergrowths. *Science, 203,* 456–458.

Veblen, D. R. and C. W. Burnham (1975) Triple-chain biopyriboles: newly discovered intermediate products of the retrograde anthophyllite–talc transformation, Chester, Vermont. *EOS, 56,* 1076.

——— and ——— (1976) Biopyriboles from Chester, Vermont: the first mixed-chain silicates. *Geol. Soc. Am. Abstracts with Programs, 8,* 1153.

——— and ——— (1978a) New biopyriboles from Chester, Vermont: I. Descriptive mineralogy. *Am. Mineral., 63,* 1000–1009.

——— and ——— (1978b) New biopyriboles from Chester, Vermont: II. The crystal chemistry of jimthompsonite, clinojimthompsonite, and chesterite, and the amphibole–mica reaction. *Am. Mineral., 63,* 1053–1073.

——— and P. R. Buseck (1977) Petrologic implications of hydrous biopyriboles intergrown with igneous pyroxene. *EOS, 58,* 1242.

——— and ——— (1978) Retrograde hydration reactions in biopyriboles. *Geol. Soc. Am. Abstracts with Programs, 10,* 509.

——— and ——— (1979a) Chain-width order and disorder in biopyriboles. *Am. Mineral., 64,* 687–700.

——— and ——— (1979b) Serpentine minerals: Intergrowths and new combination structures. *Science, 206,* 1398–1400.

———, ——— and C. W. Burnham (1977) Asbestiform chain silicates: new minerals and structural groups. *Science, 198,* 359–365.

Wadsley, A. D. and S. Anderson (1970) Crystallographic shear, and the niobium oxides and oxide fluorides in the composition region MX_x, $2.4 < x < 2.7$. In J. D. Dunitz and J. A. Ibers, Eds., *Perspectives in Structural Chemistry III,* p. 1–58. Wiley, New York.